DEVELOPMENT OF STABILITY INDICATING METHOD OF RIOCIGUAT

8.1. SELECTION OF DRUG

Riociguat (RIO) belongs to new class of therapeutic agents called as soluble guanylate cyclase stimulators [1, 2]. Riociguat by dual mechanism of action stimulates soluble guanylate cyclase independently of nitric oxide and increases the sensitivity of soluble guanylate cyclase to nitric oxide. RIO causes increase in level of cyclic guanosine monophosphate, produces relaxation of vascular smooth muscle and antiproliferative and antifibrotic effects [3,4]. RIO is the first drug used in two forms of hypertension chronic thromboembolic pulmonary hypertension and pulmonary arterial hypertension. RIO was approved by USFDA in 2013. It is available as Adempas by Bayer Healthcare pharmaceuticals [5]. The dose of RIO is staring from 0.5 mg thrice daily [6]. It is approved by CDSCO in 2017. In India it is marketed as Riopah by Lupin Pharmaceuticals Ltd. It is not official in any pharmacopeia. Literature review reveals that there are no reports on stability indicating method development, identification and characterization of degradation products of RIO. Aim of the present work was to develop stability indicating method, identify and characterize the degradation products, isolate the major degradation products and further characterize the degradants by mass, NMR and I.R. spectral techniques.

8.2. DRUG PROFILE

Drug category: Antihypertensive [1]

General Properties

IUPAC name: methyl N-[4,6-diamino-2-[1-[(2-fluorophenyl)methyl]pyrazolo[3,4-b]pyridin-3-yl]pyrimidin-5-yl]-N-methylcarbamate [2]

Molecular Formula: $C_{20}H_{19}FN_8O_2$

Molecular Weight: 422.42g

Log P : 2.44

pKa: 4.04± 0.02

Solubility: Acetonitrile, Methanol, Dimethyl formamide, Dimethylsulphoxide

Marketed Formulation: It is marketed as RIOPAH tablet 0.5 mg by Lupin Pharma Ltd.

Mechanism of action: Riociguat is a stimulator of soluble guanylate cyclase (sGC), an enzyme in the cardiopulmonary system and the receptor for nitric oxide (NO). Riociguat increases the affinity of sGC to endogenous NO, there is increase in formation of cyclic Guanylate Mono Phosphate (cGMP) and there is vasodilatation in vascular muscle cells and reduction of pulmonary hypertension.

8.3. LITERATURE REVIEW

- *Method development and validation of ultraviolet-visible spectroscopic method for the estimation of assay of sugammadex sodium, apremilast, riociguat, and vorapaxar sulfate drugs in active pharmaceutical ingredient form by Chakravorthy AV et. al. [7]*

UV-visible spectrophotometric method was developed for the quantitative estimation of drugs- Sugammadex sodium, apremilast, RIO and vorapaxar sulphate. The method is based on measurement of absorption at maximum wavelength of 210, 230, 323 and 271 nm with water and methanol as diluents. The method was validated as per ICH guidelines. The developed method linear in the range of 33-167% for sugammadex sodium and apremilast drug substances, 50-150% for RIO and vorapaxar sulphate drug substances. The % recoveries were found to be in the range of 99.7%-100.9%for sugammadex sodium, 99.3-100.3% for apremilast, 99.7-100.3% for RIO and in the range of 99.5-100.3% for vorapaxar sulphate at different concentration levels. For precision, %RSD were found to be less than 2%.

- *Development and validation of reverse-phase high-performance liquid chromatography method for quantitative estimation of riociguat in tablet dosage form by Temigire P et. al. [8]*

RP-HPLC method was developed for quantitative determination of RIO in bulk as well as tablet form. Method was developed on Inertsil ODS-3 C 18 column (250mmX 4.6mm X 5µm) with mobile phase 0.2% trifluroacetic acid and acetonitrile in the ratio of 60: 40. The detection was performed at 254nm with flow rate of 1mL/min. Retention time of RIO was 5.26 min. The method was validated as per guidelines by ICH.

- *Analytical method development and validation for the determination of Riociguat in their formulations by LC-MS/MS by Meynathan SN et. al. [9]*

LC-MS/MS method was developed for quantitative determination of RIO using electro spray ionization in a positive mode. The method was developed on Zorbax (50 mm X 4.6mm X 5 µm) column. Mobile phase composed of 0.1% formic acid : acetonitrile (15 : 85). Flow rate was maintained at 0.5 mL/min. RIO was linear in the range of 10 to 110 ng/mL with correlation coefficient of 0.9994. The method developed was validated as per guidelines by ICH.

- *Determination of Riociguat and its major human metabolite M-1 in human plasma by stable-isotope dilution LC-MS/MS by Gnoth MJ et al. [10]*

An isotope dilution LC-ESI-MS/MS method was developed for simultaneous determination of RIO and M-1 in lithium heparanized human plasma. The method was validated as per ICH guidelines. The method showed linearity in the concentration ranging from 0.5 µg/L (LLOQ) to 100µg/L (ULOQ) for both analytes. The method was selective, specific, sensitive and highly reproducible and robust for the analysis of large number of samples.

8.4. SECTION - A

DEVELOPMENT AND VALIDATION OF STABILITY INDICATING HPLC METHOD

8.4.1. EXPERIMENTAL

8.4.1.1. Chemicals and Reagents

- RIO bulk was purchased from Angene Chemical Ltd, China.
- RIOPAH tablets were purchased from local pharmacy.
- HPLC grade Acetonitrile, acetic acid was purchased from Rankem Pvt. Ltd. Mumbai.
- Hydrochloric acid (HCl), sodium hydroxide (NaOH), hydrogen peroxide H_2O_2) were purchased from S.D. Fine Chemical Ltd. Mumbai.
- 0.22 µm Nylon 6,6 membrane filter , Ultipore® N,66® for filtration of mobile phase was procured from Pall Life Sciences ,USA.

- 0.45 µm Nylon 6,6 syringe filter for sample filtration was procured from Pall Life Sciences , USA.

8.4.1.2. Equipments and Instruments

- Equipments and Instruments utilized in the present study are same as those mentioned in section 3.4.1.2.
- Design Expert® 7.0.0 software (DX® 7.0.0) was to obtain DoE design matrix for robustness study.

8.4.1.3. Chromatographic conditions

Ammonium acetate buffer (10 mM) was prepared by dissolving 770 mg of ammonium acetate in 1000 mL double distilled water. pH of buffer was adjusted to 5.7 with acetic acid. Mobile phase was acetate buffer and acetonitrile with ratio 70: 30. Analysis was performed on Waters Symmetry C 18 column (150mm x 4.6 mm i.d. x 3.5 µm particle size).Detection was performed at 254 nm. Flow rate was maintained at 1mL/min. The injection volume was 20µL.

8.4.1.4. Preparation of Standard solution

RIO standard solution (1mg/mL) - 25 mg of RIO was weighed accurately and transferred to 25 mL volumetric flask, dissolved in acetonitrile and volume was made up to the mark with acetonitrile .

Working standard solutions were prepared in mobile phase to produce concentration in the range of 5-160 µg/mL with respect to RIO.

8.4.1.5. Preparation of forced degradation sample

Since RIO was insoluble in stressors (HCl, NaOH, hydrogen peroxide), so to conduct forced degradation study, stock solution of RIO (1mg/mL) was prepared in water: acetonitrile (50: 50).

8.4.1.5.1. Acid degradation

5 mL of RIO stock solution was transferred to 10 mL of volumetric flask, to this was added 5 mL of 1 M HCl. The solution was heated at 80ºC for 12 hrs. From this 2 mL was withdrawn and neutralized with 2 mL of 1 M NaOH and volume was made up to 10 mL with mobile phase to make the concentration of 100µg/mL. The solution

was filtered through 0.45 µ Nylon 6, 6 syringe filter before injecting into HPLC system.

8.4.1.5.2. Alkaline degradation

5 mL of RIO stock solution was transferred to 10 mL of volumetric flask, to this was added 5 mL of 0.5 M NaOH. The solution was heated at 60ºC for 3 hrs. From this 2 mL was withdrawn and neutralized with 2 mL of 0.1 M HCl and volume was made up to 10 mL with mobile phase to make the concentration of 100µg/mL. The solution was filtered through 0.45 µ Nylon 6, 6 syringe filter before injecting into HPLC system.

8.4.1.5.3. Neutral hydrolysis degradation

5 mL of RIO stock solution was transferred to 10 mL of volumetric flask, to this was added 5 mL of water. The solution was heated at 80ºC for 12 hrs. From this 2 mL was withdrawn and volume was made up to 10 mL with mobile phase to make the concentration of 100µg/mL before injecting into HPLC system.

8.4.1.5.4. Oxidative degradation

5 mL of RIO stock solution was transferred to 10 mL of volumetric flask, to this was added 5 mL of 10 % hydrogen peroxide. The solution was kept at room temperature for 2 hrs. From this 2 mL was withdrawn and volume was made up to 10 mL with mobile phase to make the concentration of 100µg/mL. The solution was filtered through 0.45 µ Nylon 6, 6 syringe filter before injecting into HPLC system.

8.4.1.5.5. Dry heat degradation

For dry heat degradation, 50 mg of RIO was spread in Petridish and kept in oven at 80ºC for 11 days. From this, 10 mg of RIO was transferred to 10 mL of volumetric flask, dissolved in water: acetonitrile (50:50) to make concentration of 1mg/mL. From this, concentration of 100 µg/mL of solution was prepared and injected into HPLC system.

8.4.1.5.6. Photolytic degradation (Dry)

For photolytic degradation, 25 mg of RIO was spread in 1 mm thickness and was exposed in photolytic chamber for 11 days. From this, 10 mg of RIO was transferred to 10 mL of volumetric flask, dissolved in water: acetonitrile (50:50) to make

concentration of 1mg/mL. From this, concentration of 100 µg/mL of solution was prepared and injected into HPLC system.

8.4.1.5.7. Photolytic degradation (Solution)

For photolytic degradation in solution form, 10 mg of RIO was transferred to 10 mL of volumetric flask , volume was made 10 mL with water: acetonitrile (50 :50) and kept in photolytic chamber for 11days. From this, concentration of 100 µg/mL of solution was prepared and injected into HPLC system.

8.4.1.6. HPLC method validation

The developed method was validated as per ICH Q2B guideline.

For linearity, standard dilutions of RIO were prepared in the concentration ranging from 5 to 160µg/mL from RIO standard solution and were injected in triplicate. Linearity was determined by plotting peak area and concentration of solution. From the graph regression equation and regression coefficient was determined.

For precision, intra-day and inter-day precision were evaluated at concentration levels ranging from 5-160µg/mL (in triplicates). Peak areas corresponding to the concentration was calculated and % RSD was determined for intra-day and inter -day precision.

% Recovery was evaluated by standard addition method. Accuracy of the method was evaluated at concentration of 40µg/mL. Accuracy of method was confirmed by recovery study from formulation at 3 level of standard addition (50%, 100% and 150%). The final concentrations for accuracy were 40, 60, 80, 100µg/mL. The concentrations were analysed in triplicates. % recovery and % RSD were calculated.

Limit of detection and limit of quantitation were calculated on the basis of standard deviation of the intercept and slope of the calibration curve. LOD and LOQ were calculated using equation $3.3*(\sigma/S)$ and $10*(\sigma/S)$, where σ is the standard deviation of intercept and S is the slope of the calibration curve.

Robustness was performed by two approaches:

Classical approach (OFAT) - robustness of the method was performed by the system suitability standards and effect of the given changes in the chromatographic conditions was evaluated: pH of buffer solution ±0.2, flow rate±0.1, detector wavelength ±2, % organic in mobile phase.

QbD approach - Four fractional factorial designs (FFD) was used ($2^{\wedge 4-1}$). Full fractional designs were fractionated by exclusion of experiments to identify higher order effects and these reduced designs are known as fractional factorial design. The combinations of factor levels represent the conditions at which responses will be measure. Each experimental condition is called a run and response measurement an observation. The entire set of run is the design. Factors were varied over at levels +1 and -1 denoting the maximum and minimum level of particular factor respectively. Factors selected were pH of buffer (5.5-5.9), % organic (28-32), flow rate (0.9-1.1), wavelength (252-256) nm .Design expert software was used to predict the percentage contribution of each factor followed by ANOVA statistical analysis, graphical representation of pareto charts, perturbation plots, 3D surface plots and contour plots.

8.4.2. RESULTS

8.4.2.1. Determination of suitable wavelength

RIO solution of 10µg/mL was prepared and was scanned in the UV region of 200-400 nm and the spectrum was recorded. RIO showed strong absorbance at 254 nm which was selected as the analytical wavelength (Fig. 8.1).

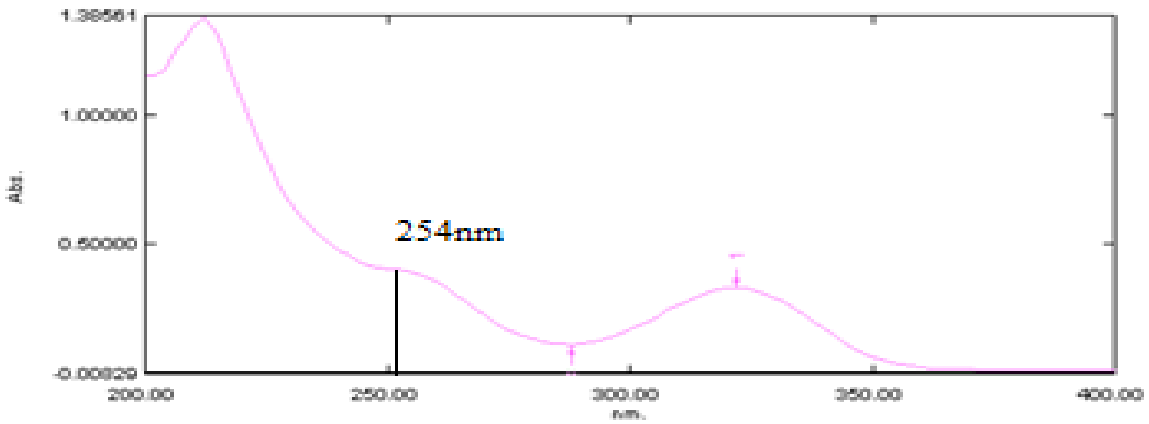

Fig. 8. 1 - Zero order spectra of RIO (10µg/mL)

8.4.2.2. Method optimisation and development

Initially for optimization, water: methanol and water: acetonitrile in various ratios were tried. With water: methanol, peak shape was broad and RIO was eluting. In force degradation study, one of the degradation products DP1 was co-eluting with

RIO. Mobile phase like 0.1% formic acid (pH 3) and ammonium formate buffer in pH 3, 4 were tried.DP1 was co eluting with RIO and both DP1 and RIO were eluting fast. Ammonium acetate buffer in the pH range pH 4-6 were tried. 10 mM ammonium acetate with pH 5.7 was found to be suitable for resolution of DP1 from RIO and retention time of RIO. Acetonitrile was found to be better in terms of resolution and peak shape of RIO. Method was developed with mobile phase containing 10 mM ammonium acetate and acetonitrile in the ratio of 70: 30 on Waters Symmetry C18 column. Flow rate was 1mL/min. Retention time of RIO is 12.44 min. Results of trials for optimisation shown in Table 8.1. The final optimised conditions for HPLC method of RIO are shown in Table 8.2 and optimised chromatogram of RIO is shown in Fig.8.2.

Table 8. 1 - Optimisation of HPLC conditions

Mobile Phase	**Ratio**	**Retention Time**	**Asymmetry**	**Theoretical Plates**
Water : Methanol	40 : 60	1.47 min	0.66 (broad peak)	1638
Water : Methanol	50 : 50	3.76 min	1.08	1821
Water :Methanol	60 : 40	4.41 min	1.02	1052
Water : Acetonitrile	50 : 50	3.37 min	1.10	4852
Water : Acetonitrile	60 : 40	4.93 min	1.08	4921
Acetate buffer pH 5.7 : Acetonitrile	65 : 35	6.85 min	1.17	6045
Acetate buffer pH 5.7 : Acetonitrile	**70 : 30**	**12.44 min**	**1.12**	**7868**

Table 8. 2 - Optimised HPLC parameters

Parameters	Optimised Value
Column	Waters Symmetry C-18 (150 x 4.6mm i.d. , 5µ particle size)
Mobile phase	Acetate buffer 10 mM pH 5.7 and acetonitrile (70: 30)
Flow rate	1.0 mL/min
Retention time	12.44±0.049 min

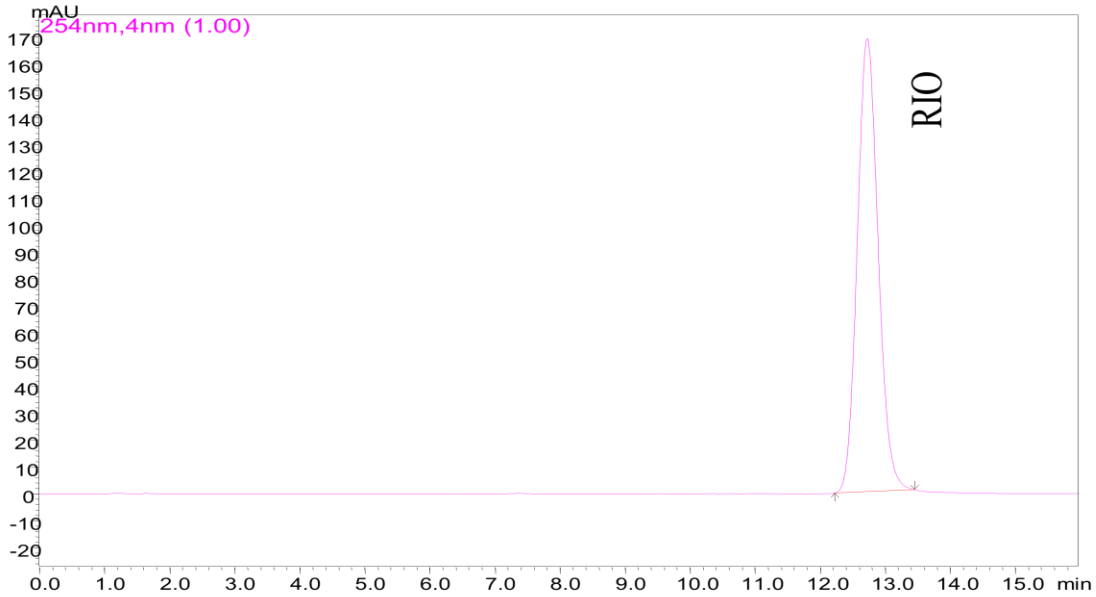

Fig. 8. 2 - Chromatogram of standard solution of RIO (100µg/mL)

8.4.2.3. Method validation using ICH Q2(R1) guideline

8.4.2.3.1. *Linearity and range*

The calibration plotted for RIO was found to be linear in the range of 5-160µg/mL. The regression equation was found to be y= 49420x- 35097 with regression coefficient (r^2) of 0.999.The linearity data is shown in Table 8.3 and calibration curve is shown in Fig. 8.3.

Table 8. 3- Linearity data of RIO

Conc. (µg/mL)	Peak Area(Mean*±%RSD)
5	283370±0.51
10	415063±0.81
20	894738.7±0.43
40	1951184±0.59
80	3956040±0.56
160	7858641±0.46

***Average of three determinants**

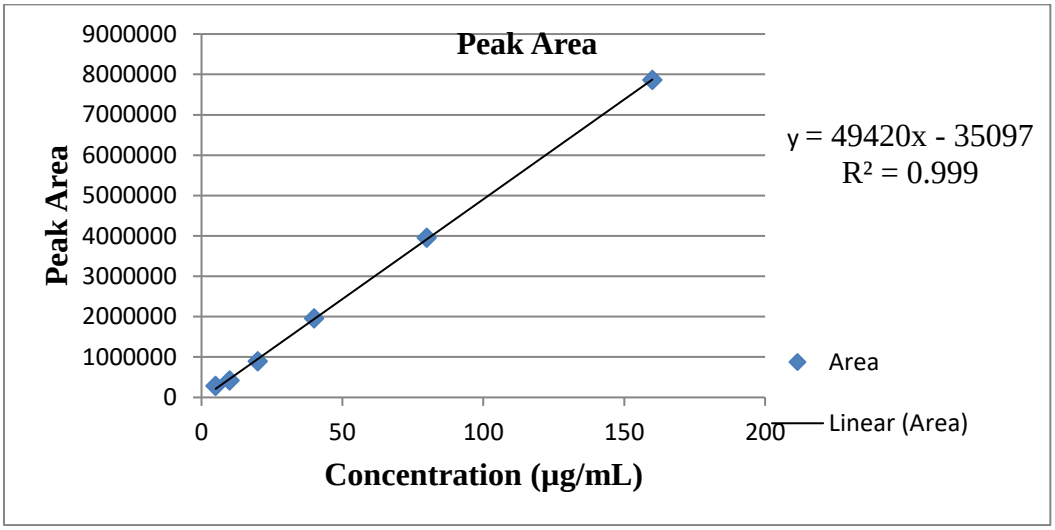

Fig. 8. 3- Calibration curve of RIO [Peak Area versus Conc. (µg/mL)]

8.4.2.3.2. *Precision*

Intra-day precision was performed by repeating the experiment three times in a day and inter-day precision was performed by repeating the experiments on three consecutive days. The average %RSD of intra-day and inter-day were found to be 1.22 and 1.41. The developed method was found to be precise (Table 8.4 and 8.5).

Table 8. 4 - Intraday Precision of RIO

Conc.(µg/mL)	Peak Area				
	Set 1	Set 2	Set 3	Mean	%RSD
5	282471	288789	282494	284585	1.27
10	414975	407516	415385	412625	1.07
20	892698	870568	890376	884547	1.37
40	1952115	1910356	1938510	1933660	1.10
80	3955061	3849245	3918562	3907623	1.37
160	7859260	7982845	7801745	7881283	1.17
				Average	1.22

Table 8. 5- Interday Precision of RIO

Conc.(µg/mL)	Set 1	Set 2	Set 3	Mean	%RSD
5	282471	284678	290587	285912	1.46
10	414975	403876	415346	411399	1.58
20	892698	889214	909267	897059.7	1.19
40	1952115	1894865	1902647	1916542	1.62
80	3955061	3833586	3909853	3899500	1.57
160	7859260	7972545	7807589	7879798	1.07
				Average	1.41

8.4.2.3.3. ***Accuracy***

Accuracy of method was determined by calculating % percent recovery of the analyte recovered. To the sample concentration of 40µg/mL, standard solution of RIO was added as 50%, 100% and 150% to give concentrations as 60, 80, 100 µg/mL. Recovery greater than 99% indicates the developed method was accurate (Table 8.6).

Table 8. 6- Accuracy data of RIO

Excess drug added to analyte (%)	**Theoretical Content (µg/mL)**	***Amount Found (µg/mL)**	**%Recovery±SD**
0	40	40.23	100.58±0.62
50	60	59.89	99.45±0.30

100	80	80.05	100.05±0.36
150	100	100.08	100.13±0.80

*Average of three determinations

8.4.2.3.4. ***Limit of detection and limit of quantification***

LOD and LOQ were found to be 0.046 µg/mL and 0.139 µg/mL.

8.4.2.3.5. ***Robustness***

(i) Classical approach **-** For robustness study, slight changes were made in chromatographic conditions e.g. pH of buffer, flow rate, % organic and wavelength. The results were expressed as % RSD. % RSD less than 2 indicated that the developed method was robust (Table 8.7).

Table 8. 7- Robustness data of RIO

Factor	Levels	Area		Retention Time		Tailing Factor		Theoretical Plates	
		Mean	%RSD	Mean	%RSD	Mean	%RSD	Mean	%RSD
pH	5.5	1674727	1.33	12.45	0.34	1.12	0.27	7864.33	0.007
	5.7	1657713	1.21	12.52	0.26	1.12	0.1	7863.33	0.019
	5.9	1655378	1.04	12.44	0.48	1.12	0.18	7863.66	0.019
Flow Rate	0.9	1649302	1.26	12.94	0.19	1.14	0.35	7862.66	0.01
	1	1670357	1.21	12.53	0.2	1.13	0.23	7862.66	0.03
	1.1	1617963	1.24	12.84	0.21	1.15	0.45	7863.33	0.01
% Organic	28	1682940	1.06	12.84	0.29	1.14	0.17	7863.33	0.01
	30	1672367	0.96	12.55	0.16	1.13	0.17	7863	0.03
	32	1674304	1.11	12.28	0.16	1.12	0.18	7862.66	0.01
Wavelength	252	1679118	1.04	12.62	0.19	1.13	0.13	7864.33	0.01
	254	1654959	1.21	12.54	0.24	1.12	0.13	7863.33	0.03
	256	1683539	0.59	12.64	0.24	1.12	0.18	7863.33	0.01

(ii) QbD approach - Fractional factorial method DoE was performed for robustness study. Factors for fractional factorial design and obtained responses are summarized in Table 8.8. Design matrix composed of $2^{\wedge 4-1}$ with factors were varied over two levels that is minimum and maximum. Four parameters selected were pH of buffer, % organic, flow rate, wavelength. Four critical quality attributes taken were retention time, area, tailing factor and number of the theoretical plates.

Table 8. 8- Fractional factorial design for robustness testing using factors and obtained responses.

Factors				**Responses**			
A: pH	B: % Organic	C: Flow rate	D: wavelength	Retention Time	Area	Tailing Factor	Theoretical Plates
5.9	32	0.9	252	12.95	1682854	1.12	7863
5.5	32	1.1	252	12.54	1685283	1.11	7864
5.5	28	0.9	252	12.94	1683827	1.09	7864
5.5	28	1.1	256	12.52	1682742	1.12	7863
5.5	32	0.9	256	12.94	1683823	1.11	7863
5.9	28	1.1	252	12.62	1683826	1.11	7864
5.9	32	1.1	256	12.48	1682384	1.12	7864
5.9	28	0.9	256	12.98	1684721	1.11	7864

Among the various models, polynomial model was suggested by the design with the highest least square regression value for all responses as compared to other models. The model was examined using lack of fit test, which indicated insignificant lack of fit value corresponding with higher p-value as compared to the model F-value. Graphical interpretation in the form of pareto charts, perturbation plots, 3-D response plot and contour plot showed the correlation of effect of factors on the response's retention time, area, tailing factor and theoretical plates of RIO.

Pareto charts and perturbation indicated (Fig. 8.4 a-d and Fig. 8.4e-h) that none of the factors had significant effect on responses. The model was evaluated for the effect of individual factors on the responses in the form of 3-D response surface plots and contour plots. 3-D response surface plots and contour plots indicated that the effect of

all the responses are independent of the factors pH, % Organic, flow rate and theoretical plates (Fig. 8.5 a-d and Fig. 8.5 e-h).

(a) Pareto charts (Retention time)

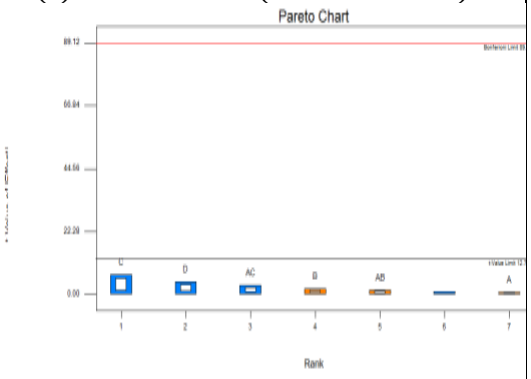

(e) Perturbation plot (Retention time)

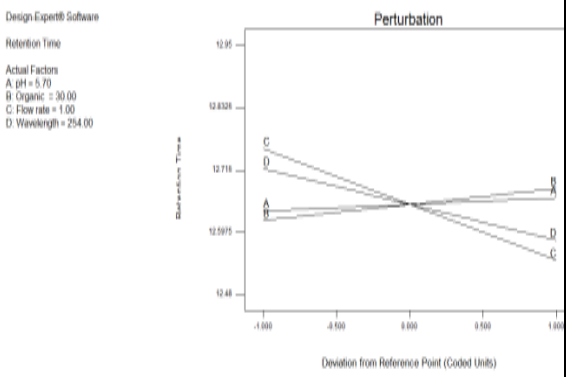

(b) Pareto charts (Area)

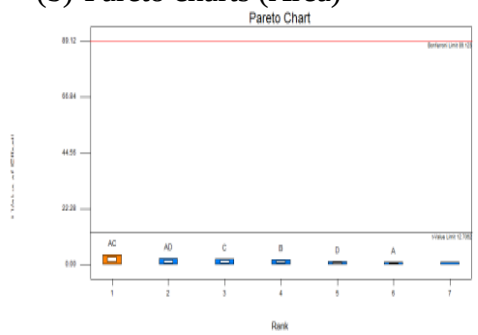

(f) Perturbation plot (Area)

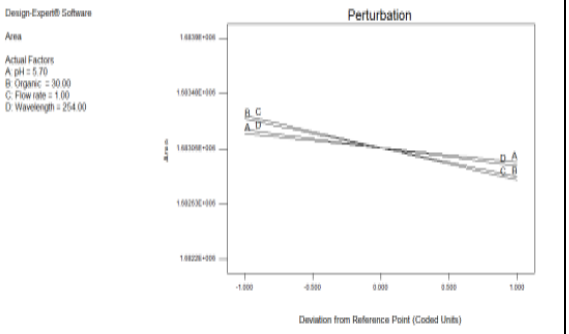

(c) Pareto charts (Tailing Factor)

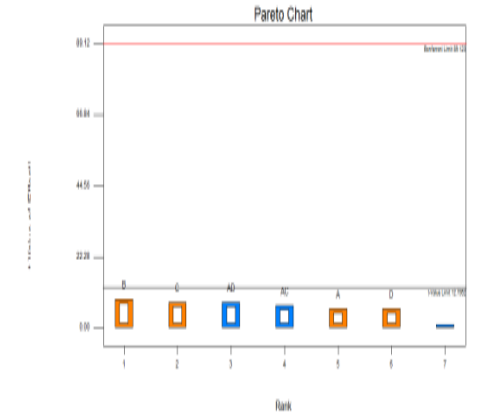

(g) Perturbation plot (Tailing Factor)

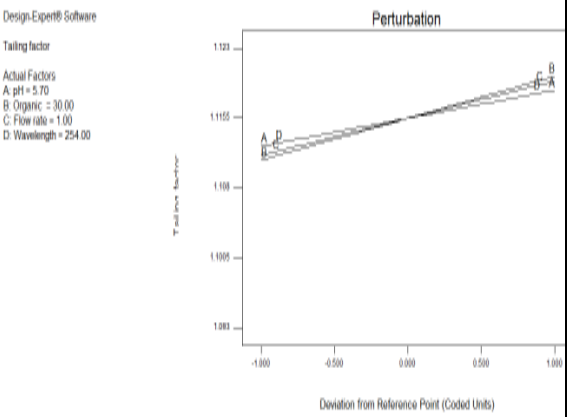

(d) Pareto charts (Theoretical Plates)

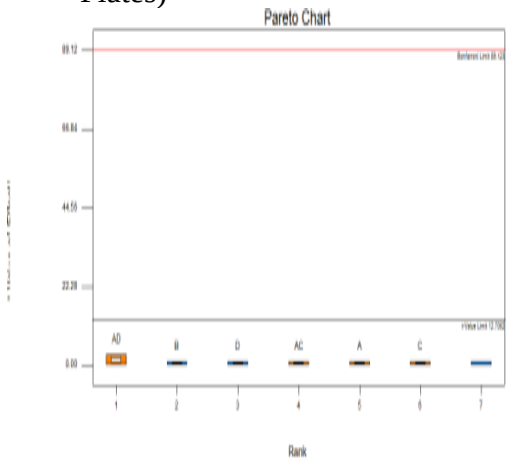

(h) Perturbation plot (Theoretical Plates)

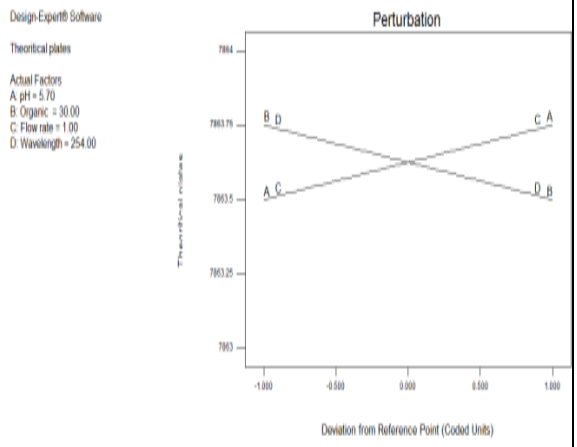

Fig. 8. 4 - Pareto charts (a-d) and perturbation plots (e-h) showing effect of factors on responses

(a) 3D- response surface plot (Retention time)

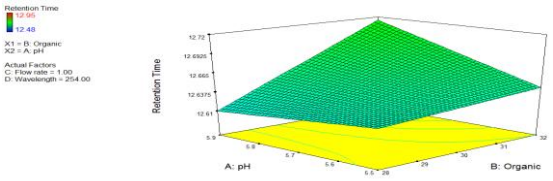

(e) Contour plot (Retention time)

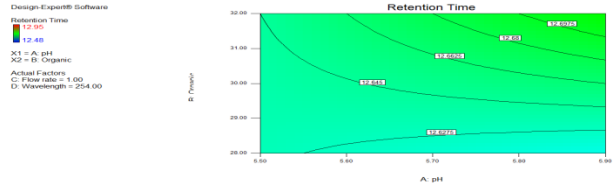

(b) 3D- response surface plot (Area)

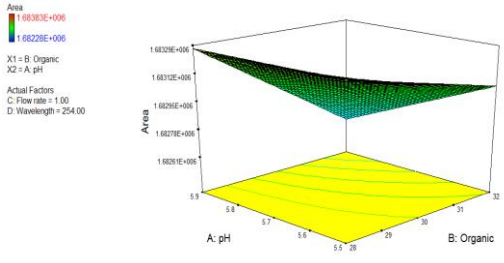

(f) Contour plot (Area)

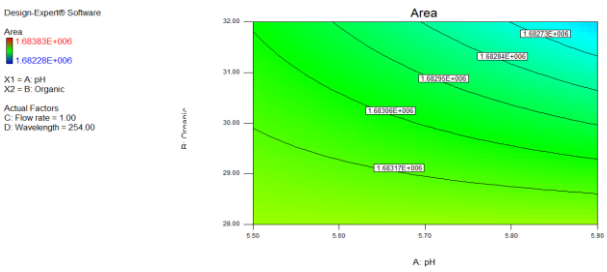

(c) 3D- response surface plot (Tailing Factor)

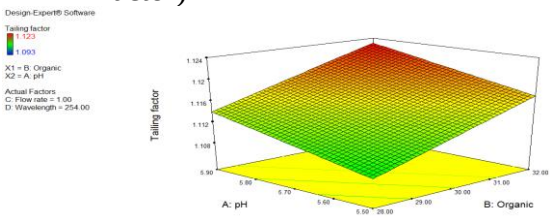

(g) Contour plot (Tailing Factor)

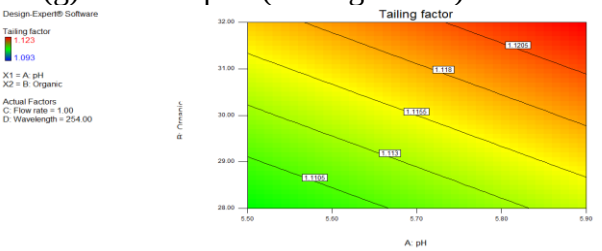

(d) 3D- response surface plot (Theoretical Plates)

(h) Contour plot (Theoretical Plates)

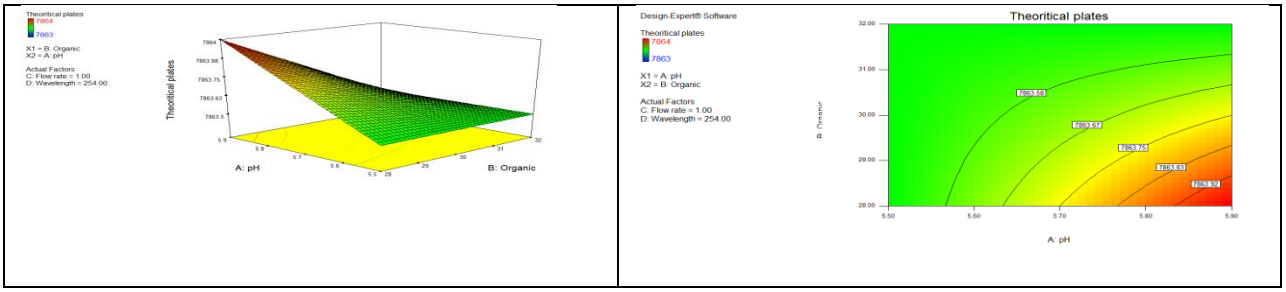

Fig. 8. 5 - 3-D response surface plots (a-d) and contour plots (e-h) showing effect of factors on responses

Further model was validated by the application of analysis of variance (ANOVA) to all response variable to examine the significance of the model, which showed that all the responses achieved are insignificant differences in their values. Equations obtained from the model were as

Retention Time Y1 = +12.65 +0.012 *A -0.11* C -0.068* D -0.047 *A* C

Area Y2 = +1.683E+006-111.00* A -249.00* C -139.75* D +408.00 * A * C-254.25 * A * D

Tailing factor Y3 = +1.12 +4.500E-003 * B+4.000E-003* C

Theoretical plates Y4 = +7863.63 +0.12 *A -0.13 *B -0.13 *D +0.38 *A*D

From the equation, positive indicates synergistic effect, negative sign indicates antagonistic effect in the polynomial equation. From the table of ANOVA (Table 8.9) of response Y1, Y2, Y3 and Y4 indicates that predicted values for all the factors are under satisfactory value. Model p-value > 0.05 indicates that factors had non-signiifcant effect on the responses resulting in a robust method.

Table 8. 9 - Statistical parameters by ANOVA analysis for the responses

Parameters	SS	df	MS	F-value	p-value	Model F-value	Model p-value	Prob > F
Response Y1 (Retention Time)								
pH	0.001	1	0.0012	0.69	0.55	14.37	0.19	not significant
% Organic	0.007	1	0.0072	4	0.29			
Flow rate	0.08	1	0.0882	49	0.09			

Wavelength	0.03	1	0.0364	20.25	0.13			
Response Y2 (Area)								
pH	98568	1	98568	0.19	0.73	0.83	0.68	not significant
% Organic	393384.5	1	393384.5	0.76	0.54			
Flow rate	496008	1	496008	0.95	0.50			
Wavelength	156240.5	1	156240.5	0.30	0.68			
Response Y3 (Tailing Factor)								
pH	7.2E-05	1	7.2E-05	36	0.10	55	0.10	not significant
% Organic	0.0001	1	0.0001	81	0.07			
Flow rate	0.0001	1	0.0001	64	0.07			
Wavelength	7.2E-05	1	7.2E-05	36	0.10			
Response Y 4 (Theoretical Plates)								
pH	0.12	1	0.12	1	0.50	2.33	0.46	not significant
% Organic	0.12	1	0.12	1	0.50			
Flow rate	0.12	1	0.12	1	0.50			
Wavelength	0.12	1	0.12	1	0.50			

SS- sum of squares, df – degrees of freedom, MS- Mean square

8.4.2.3.6. *Selectivity*

Selectivity of the developed method was determined by peak purity analysis of all chromatographic peaks by using PDA detector. All peaks were well separated from each other with optimum resolution and peak purity were found to be greater than purity threshold. Hence the developed method was selectively stability indicating (Table 8.10).

Table 8. 10 - Peak purity data of RIO and degradation products

S.No.	Peaks	Rt	Peak Purity Index	Single Point threshold
1	RIO	12.44 min	0.999999	0.999949
2	DP1	11.4 min	0.999989	0.999671
3	DP2	9.4 min	0.999926	0.996598
4	DP3	4.0 min	0.999948	0.999259

8.4.2.3.7. *Stability in sample solutions*

Stock solution of RIO and stressed samples were prepared from standard stock solution and then stored at room temperature for 24 hrs. No additional peaks were observed which indicated stability of RIO sample solution.

8.4.2.3.8. *System Suitability Parameters*

System suitability tests were performed on freshly prepared solution with n=6 containing RIO. The results of system suitability parameters are shown in Table 8.11.Peak purity data of RIO is shown in Table 8.10 and peak purity curve is shown in Fig.8.8.

Table 8. 11 - System suitability parameters of RIO

Parameters	Data Obtained
Retention Time (min ± SD)	12.44 ± 0.049
Tailing Factor ± SD	1.124 ± 0.003
Theoretical Plate ± SD	7866.378 ± 372.177

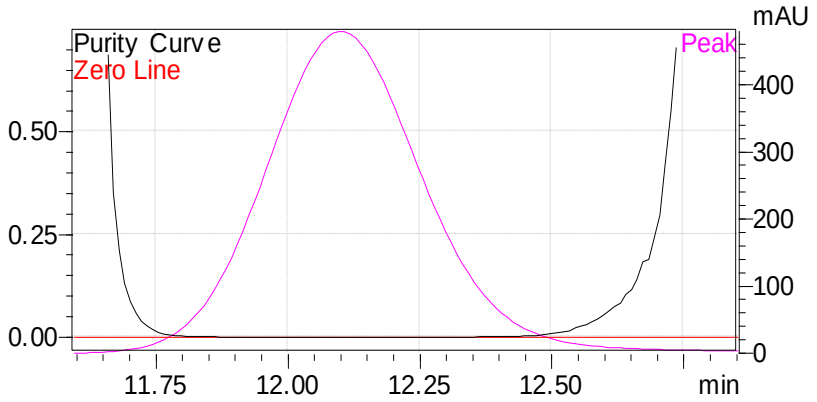

Fig. 8. 6- Peak purity curve of RIO

8.4.2.4. Stress Degradation studies

8.4.2.4.1. Acid degradation –No degradation was observed when RIO was subjected to 1M HCl at 80ºC for 12 hrs (Fig. 8.7).

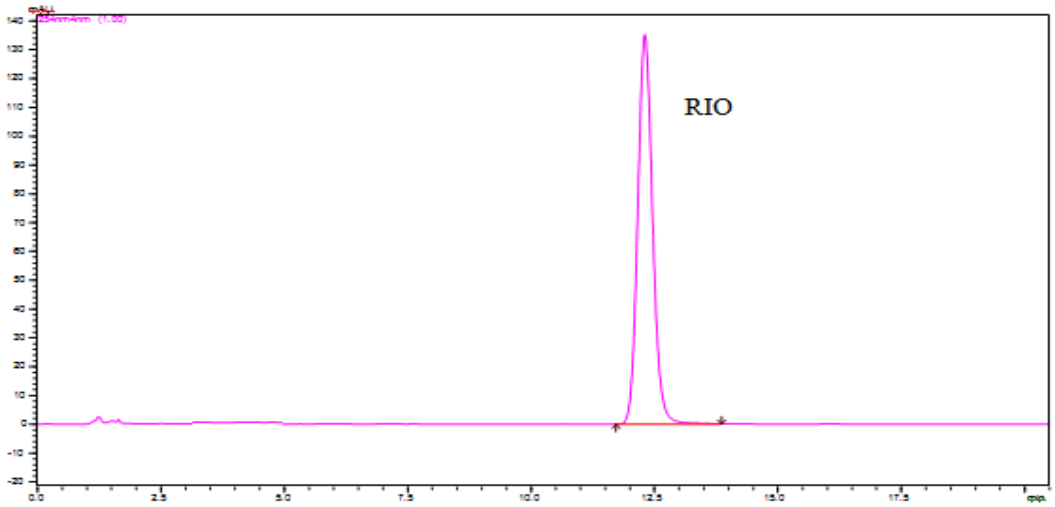

Fig. 8. 7- Chromatogram of acid degradation (API)

8.4.2.4.2. Alkaline degradation – Significant degradation (23.8%) was observed RIO was subjected to 0.5 M NaOH at 60 ºC for 3 hrs with the formation of degradation products DP1 and DP2 at retention time of 11.4 and 9.4 min (Fig. 8.8) respectively.

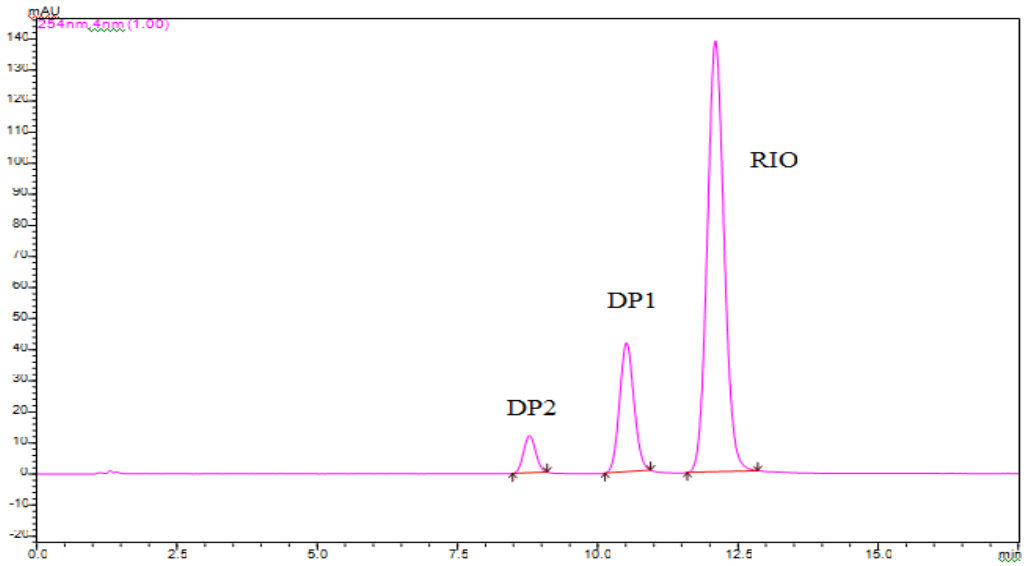

Fig. 8. 8 - Chromatogram of alkaline degradation (API)

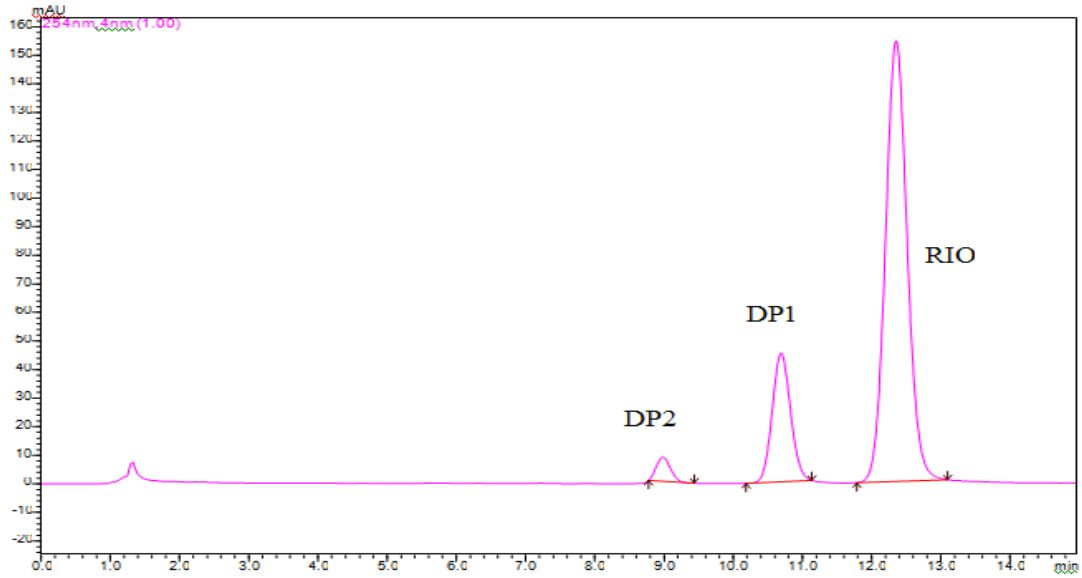

Fig. 8. 9- Chromatogram of alkaline degradation (formulation)

8.4.2.4.3. Neutral hydrolysis degradation - No degradation was observed when RIO was subjected to neutral hydrolysis at 80ºC for 12 hrs (Fig. 8.10).

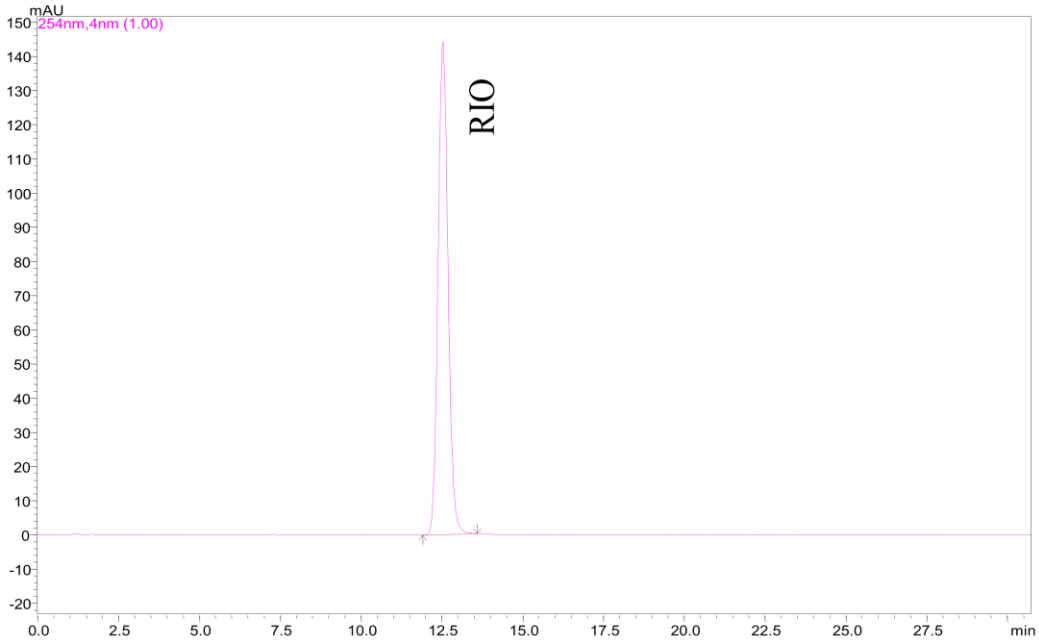

Fig. 8. 10- Chromatogram of neutral hydrolysis degradation(API)

8.4.2.4.4. Oxidative degradation- Slight degradation (9.8 %) was observed when RIO was treated with 10% hydrogen peroxide at room temperature for 2 hrs with the formation of degradation products DP3 at retention time of 4.1 min (Fig. 8.11).

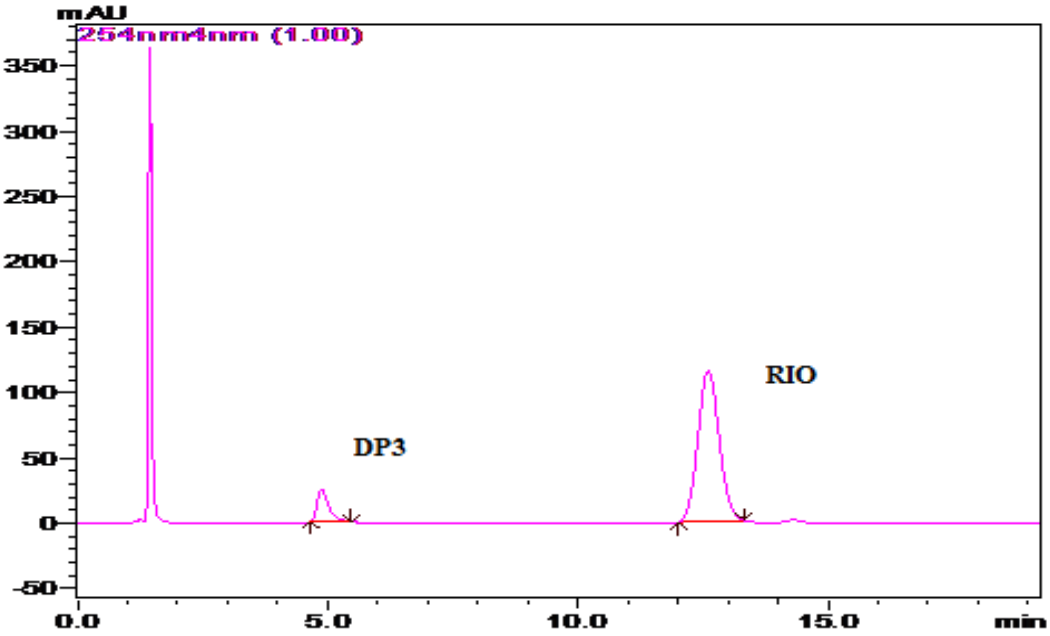

Fig. 8. 11 - Chromatogram of oxidative degradation (API)

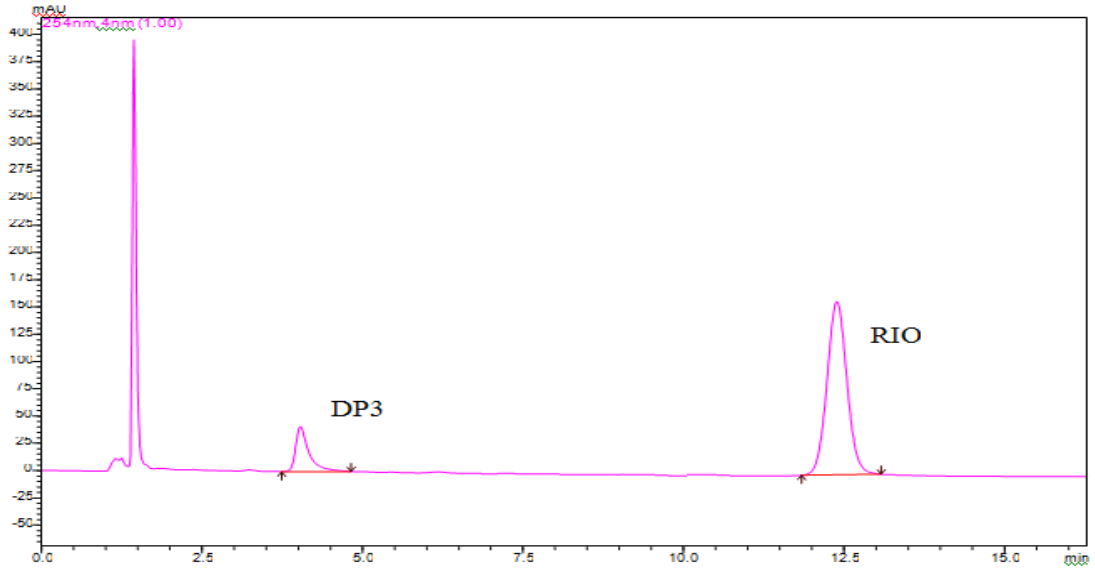

Fig. 8. 12- Chromatogram of oxidative degradation (formulation)

8.4.2.4.4. Dry heat degradation – No degradation was observed when RIO was subjected to thermal degradation at 80ºC for 11 days (Fig. 8.13).

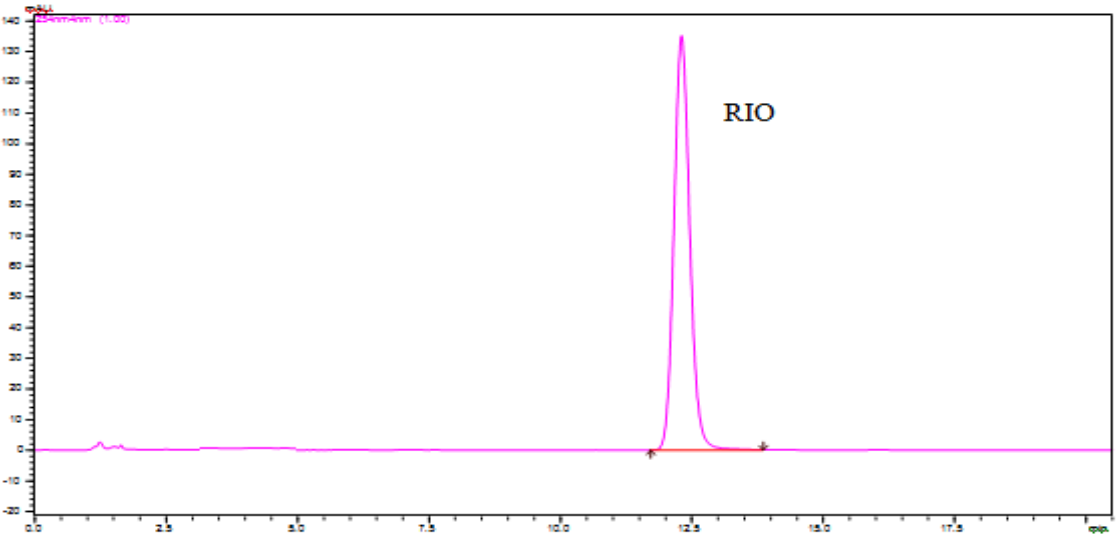

Fig. 8. 13- Chromatogram of thermal degradation

8.4.2.4.5. Photolytic degradation- No degradation was observed when RIO was subjected to photolytic degradation (dry and solution) for 11days (Fig. 8.14 and 8.15).

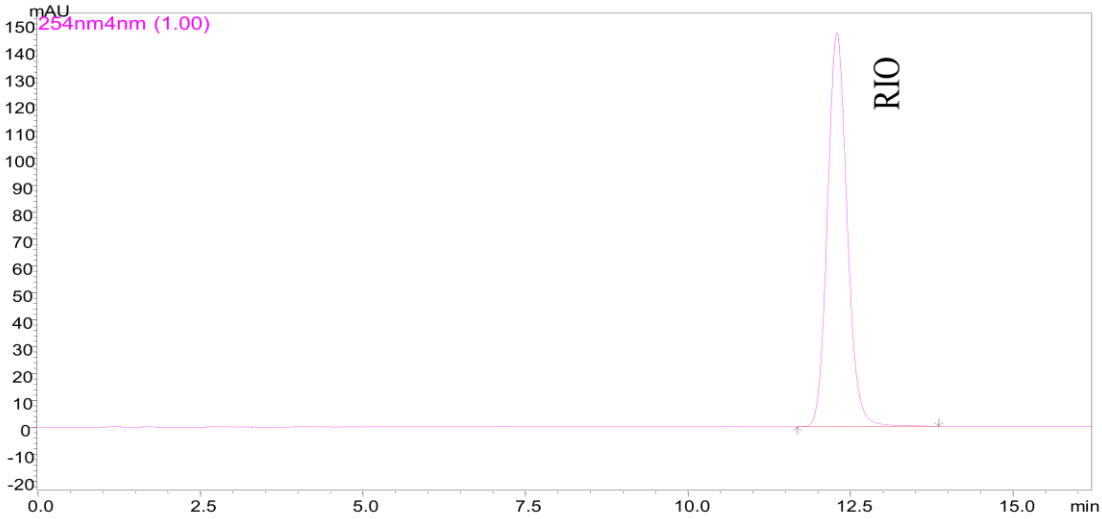

Fig. 8. 14 - Chromatogram of Photolytic degradation (Dry) (API)

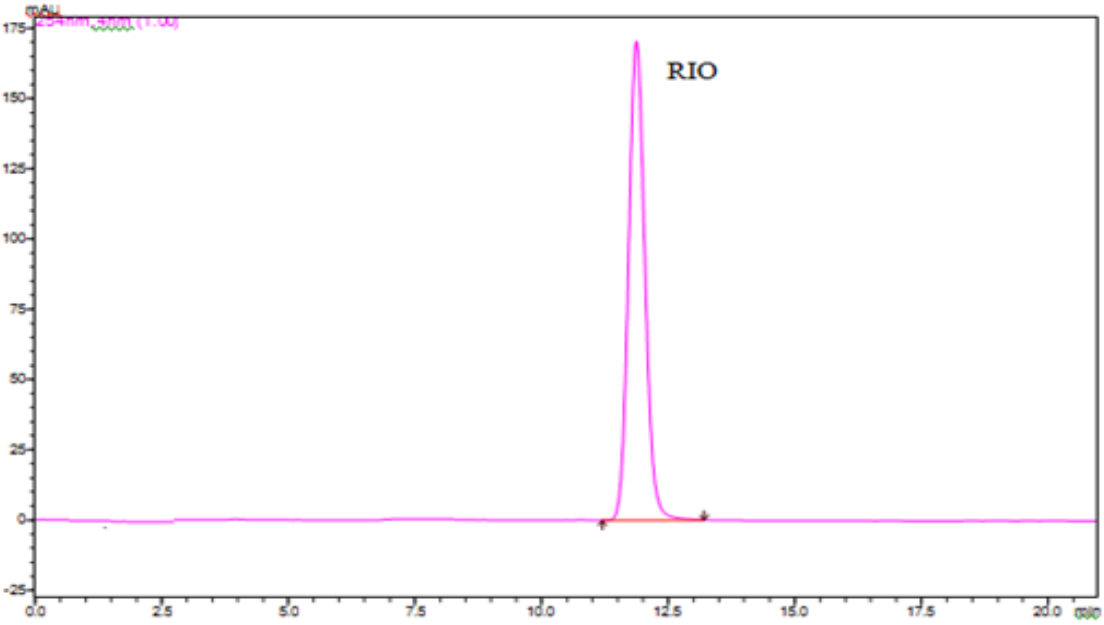

Fig. 8. 15 - Chromatogram of Photolytic degradation (Solution) (API)

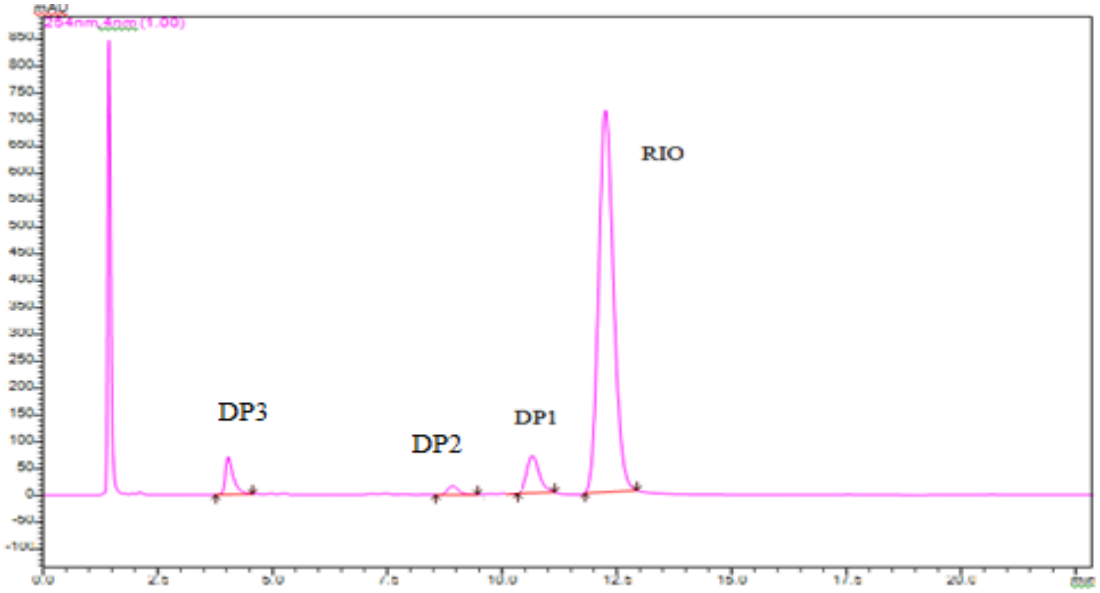

Fig. 8. 16 - Chromatogram of combined degradation products of all stressors

Table 8. 12- Summary of forced degradation study of RIO

Stress Condition	Condition	RT of Degradation Products	% of Degradation Products in API	% of Degradation products in formulation
Acid	1M HCl 80ºC for 12 hrs	---	---	---
Alkaline	0.5 M NaOH 60ºC for 3 hrs	8.9min (DP2) 11.4 min (DP1)	23.8%	22.3%
Neutral	80ºC for 12 hrs	--	--	--
Oxidative	10 % H_2O_2RT for 2 hrs	4.0 min(DP3)	9.8%	11.1%
Thermal	80ºC for 11 days	--	--	--
Photolytic Dry	5382 Lux and 144UW/cm^2 for 11 days	--	--	--
Photolytic Solution		--	--	--

8.4.2.5. Applicability of the developed method for the analysis of formulation

Forced degradation study was performed on marketed formulation. The conditions were same as mentioned for API and samples were analyzed in the same way as that of API. The chromatograms were recorded. Minor variation was observed in the % degradation of API and formulation samples as shown in Table 8.12.

8.4.3. DISCUSSIONS

Maximum absorption wavelength of 254 nm was selected as detection wavelength after scanning in the range from 200-400 nm. Various trials were taken for optimization of chromatographic procedure. With water and methanol in various ratios, peak shape was broad and RIO was eluting fast. Method was optimized with acetate buffer (pH 5.7) and acetonitrile in the ratio of 70: 30 and also for separation degradation product DP1 from RIO. Separation of degradation product DP1 from RIO was tried on acidic pH. With mobile phase 0.1 % formic acid (pH 3) and ammonium formate buffer pH (4-5), DP1 was co-eluting with RIO. DP1 was separated from RIO with acetate buffer pH 5.7. Significant degradation (23.8%) was obtained in alkaline condition and slight degradation (9.8%) was obtained in oxidative condition. RIO was stable in acidic, neutral hydrolytic, thermal and photolytic conditions as there was not any additional peak in the chromatogram and peak height of RIO was not reduced. The developed method was validated as per ICH guidelines. Good correlation was obtained between peak area and concentration of RIO in the range of 10-120 µg/mL with regression coefficient r^2 0.999. % RSD for intra-day and inter-day precision was less than 2%. % Recovery was found to be in the range of 99.11-100.05%. Both traditional approach and fractional factorial design was successfully used to test the robustness of the developed method.

8.5. SECTION - B

DEGRADATION KINETIC STUDY OF RIOCIGUAT BY HPLC METHOD

The degradation kinetics was studied for alkaline since RIO was susceptible to alkaline condition.

8.5.1. EXPERIMENTAL

8.5.1.1. Chemicals and Reagents

The chemicals and reagents used in the present section were same as those mentioned in section 8.4.1.1.

8.5.1.2. Equipments and Chromatographic Conditions

Equipments and chromatographic conditions were same as those mentioned in section 8.4.1.2.

8.5.1.3. Preparation of stock, sample and buffer solutions

Stock solution was same as those mentioned in section 8.4.1.5.

Alkaline degradation kinetics study - To the 5 ml of stock solution of in RIO in 10 ml of volumetric flask. , 5 ml of 0.1 /0.5/1.0 M sodium hydroxide was added. The solutions were kept at 60º/ 70˚C/80ºC from 1 hour to 6 hours. From this solution, 2mL was transferred to 10mL volumetric flak and neutralized with 2mL 0.1/0.5/1.0 M HCl and the solution was made up to volume with mobile phase to make the concentration 100µg/mL and injected in to the HPLC system.

8.5.2. RESULTS

Degradation rate kinetics was studied by % of drug remaining after degradation versus time (for zero order kinetics) using linear regression analysis, Log of % drug remaining after degradation (for first order process). Experiments were performed in triplicate and average values were taken for analysis. The rate constant (K), half-life ($t_{1/2}$) and activation energy (Ea) were calculated from slope of line at each temperature for alkaline degradation.

A regular decrease in concentration of RIO was observed with increasing time intervals and with increase in temperature. Regression equation and regression coefficient was obtained for zero order and first order kinetics for different concentration of sodium hydroxide and at different temperatures. On the basis of regression, degradation follows first-order kinetics since r^2 values are highest (close to 1) (Table 8.13).

On the basis of first-order kinetics, further study was performed to study the effect of temperature on the rate constant the Arrhenius plots were plotted (log of rate constant versus reciprocal of temperature). Arrhenius equation as

$$\log K = \log A - Ea/2.303\ RT$$

where K is the rate constant, A is the frequency factor, Ea is the activation energy, R is the gas constant (1.987 cal/deg/mol) and T is the absolute temperature. Arrhenius plot was obtained by plotting lnK versus 1/T. Graph was linear in the temperature range. The first order kinetic plot and Arrhenius plot for alkaline degradation are shown in Fig 8.17 -8.22. The values of degradation rate constant, half-life and activation energy are shown in Table 8.14.

Table 8. 13- r^2 value and Regression Equation for zero order, first order reaction for alkaline degradation

S.No.	Conc. NaOH	Temp	r^2		Regression equation	
			Zero order	First Order	Zero order	First Order
1	0.1M	60ºC	0.979	0.980	y=-2.614x+ 98.9	y=-0.012x+1.996
		70˚C	0.969	0.978	y=-5.576x+97.06	y=-0.030x+1.994
		80˚C	0.979	0.994	y=-7.354x+91.34	y=-0.048x+1.979
2	0.5M	60ºC	0.963	0.988	y= -8.7x+82.1	y=-0.073x+1.951
		70˚C	0.792	0.868	y=-5.968x+61.78	y=-0.083x+1.803
		80˚C	0.969	0.996	y=-5.477x+45.48	y=-0.092x+1.716
3	1.0 M	60ºC	0.955	0.994	y=-6.577x+55.05	y=-0.090x+1.795
		70˚C	0.903	0.992	y=-6.674X+50.03	y=-0.111x+1.773
		80˚C	0.964	0.996	y=-5.14x+38.28	y=-0.115x+1.665

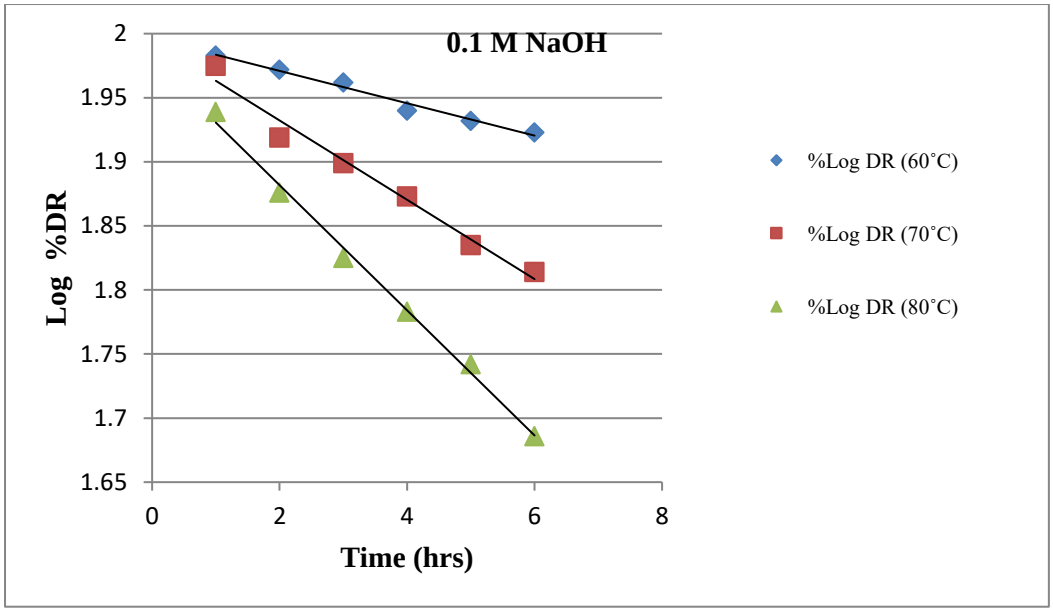

Fig. 8. 17- First order reaction kinetics of 0.1 M NaOH

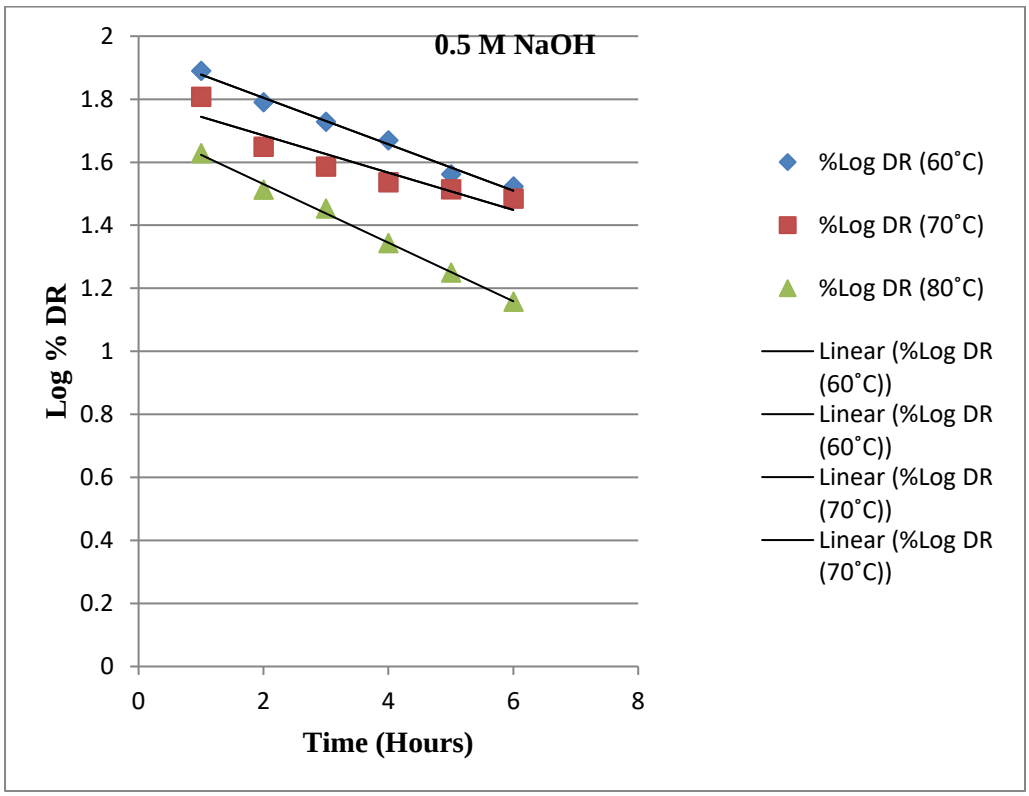

Fig. 8. 18- First order reaction kinetics of 0.5 M NaOH

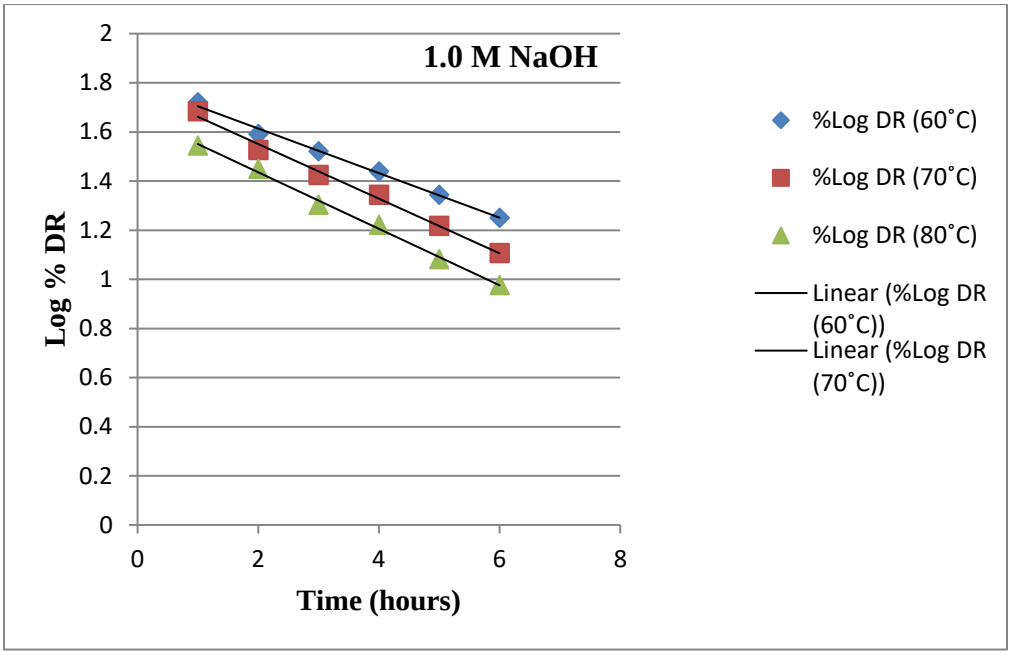

Fig. 8. 19- First order reaction kinetics of 1.0 M NaOH

Table 8. 14- Degradation rate constant, half-life and Activation Energy Ea for first order kinetic of alkaline degradation

S.No.	Conc. NaOH	Temp	K	$t_{1/2}$ (hrs)	Activation energy (Ea)
1	0.1 M	60ºC	0.0276	25.07	7.263 KJ/mole
		70˚C	0.0690	10.03	
		80˚C	0.1105	6.26	
2	0.5M	60ºC	0.1681	4.12	
		70˚C	0.1911	3.65	
		80˚C	0.2141	3.23	
3	1.0 M	60ºC	0.2072	3.34	
		70˚C	0.2556	2.71	
		80˚C	0.2648	2.61	

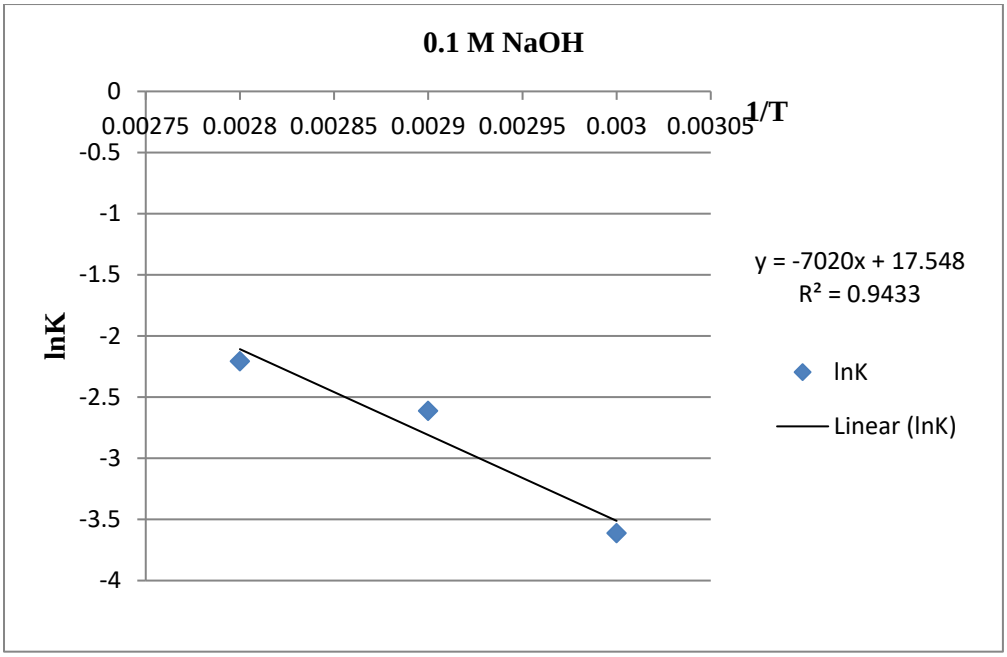

Fig. 8. 20- Activation energy plot for 0.1 M NaOH

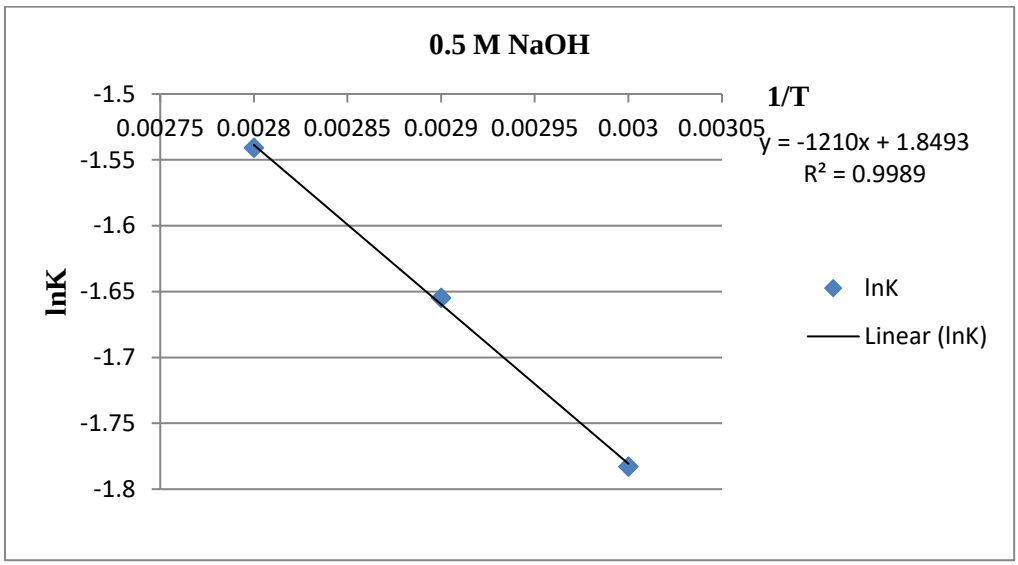

Fig. 8. 21- Activation energy plot for 0.5 M NaOH

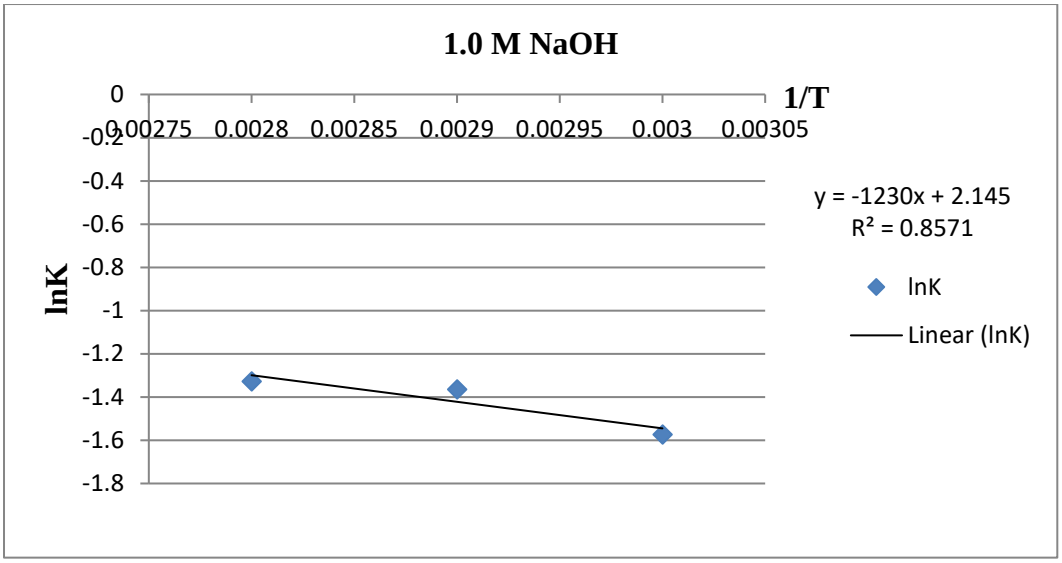

Fig. 8. 22- Activation energy plot for 1.0 M NaOH

8.5.3. DISCUSSIONS

Degradation kinetics was studied for alkaline conditions.

For alkaline degradation kinetics, factors taken for kinetics study were: concentration sodium hydroxide (0.1 M, 0.5 M and 1.0 M), temperature (60º, 70ºand 80º C), time (1 hr to 6 hrs) . Zero order kinetics study was performed by plotting graph between % drug remaining versus time and first order by plotting graph between log % Drug remaining versus time. Regression equation and regression coefficient were obtained for both zero and first order kinetics. Degradation follows first-order kinetics since regression coefficient r^2 *was* highest in first –order kinetics. Based on this degradation rate constant and half-life was calculated. After plotting lnk (rate constant) versus 1/T, activation energy calculated which was found to be 7.263 KJ/mole.

8.6. SECTION - C

ISOLATION AND CHARACTERIZATION OF MAJOR DEGRADATION PRODUCTS OF RIOCIGUAT

8.6.1. EXPERIMENTAL

8.6.1.1. Chemicals and Reagents

Chemicals and reagents used in the present section are same as those mentioned in section 8.4.1.1.

8.6.1.2. Equipments and chromatographic conditions

Preparative HPLC system composed of Shimadzu LC-20 AP pump and SPD 20A detector. Separation was performed on Promosil column (250X 50 mm, 10µ). Detection was performed at 254 nm. Flow rate was maintained at 55 mL/min. Sample was injected though Rheodyne 7725 injector valve. Data acquisition and integration was processed with Class VP software. The gradient programme was (time/% B): 0/30, 45/35, 46/100, 50/100, 55/30, 60/30.

Attached proton test in ^{13}CNMR was performed , indicated presence of quaternary carbon and methylene as negative peaks, methyl and methine groups as positive peaks.

LC-MS/MS analysis was performed using Q-Extractive plus Biopharma High Resolution Orbitrap Liquid Chromatograph Mass Spectrophotometer (Thermo Fischer Pvt. Ltd) equipped with electro spray ionization source in a positive mode. Xcalibur software was used for mass spectroscopic studies.

Major degradation products were DP1, DP2 obtained in alkaline hydrolysis and DP3 in oxidative condition respectively.

8.6.1.3. Enrichment of degradation samples DP1, DP2 and DP3

To collect sufficient quantity of DP1, DP2 and DP3, 1 g of RIO was subjected to alkaline and oxidative degradation conditions. The samples were analysed as described in section 8.4.1.5.2. and 8.4.1.5.4. DP1 and DP2 are formed with 50% and 15% by area normalization (Fig. 8.23) and in oxidative condition DP3 is formed with 10% by area normalization (Fig. 8.24).

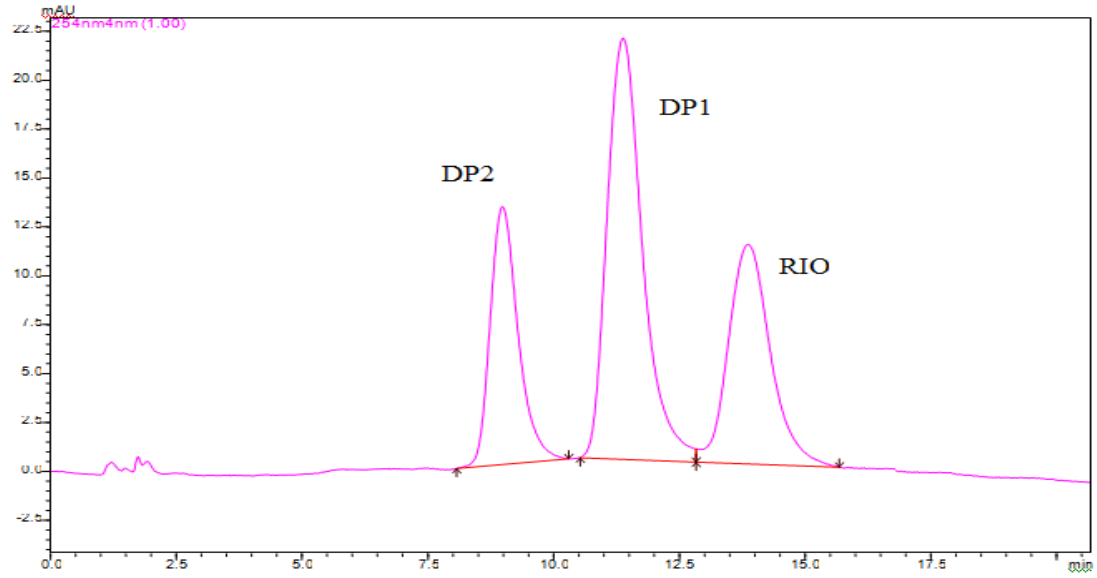

Fig. 8. 23 - Chromatogram of alkaline condition

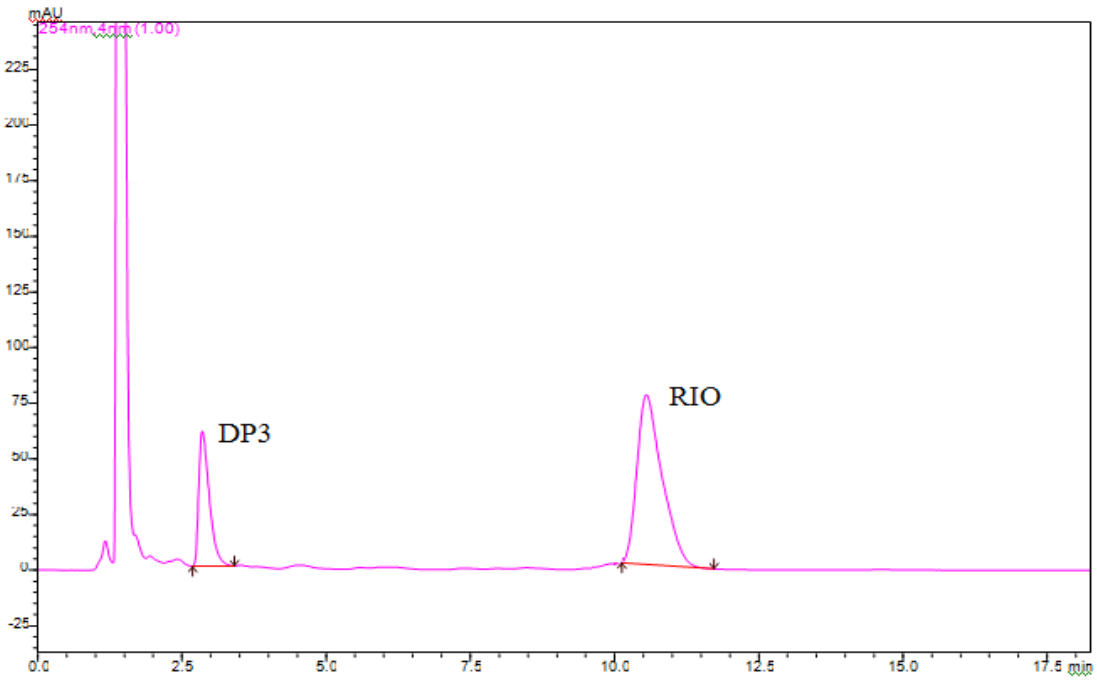

Fig. 8. 24- Chromatogram of oxidative condition

8.6. 1.3. Isolation of degradation products by preparative HPLC

Fractions of DP1-DP3 greater than 95% were collected together. Acetonitrile was removed by concentrating the solution on rotary vapour. The retention time and purity of isolated fractions were confirmed by analytical HPLC as mentioned in 8.4.1.5.2. and 8.4.1.5.4. The solutions were kept in lyophilizer overnight. DP1 was obtained as yellow solid while DP2 and DP3 were obtained as white solids. % purity

of DP1, DP2 and DP3 were obtained as 99.6, 99.3 and 99.1% respectively. Chromatograms of isolated DP1, DP2 and DP3 are shown in (Fig. 8.25).

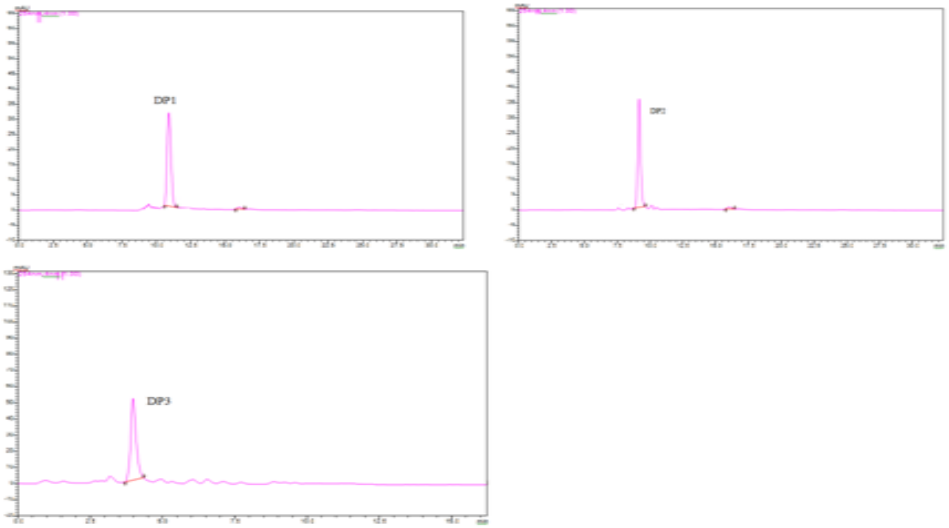

Fig. 8. 25 - Chromatograms of isolated DP1, DP2 and DP3

8.6.2. RESULTS

8.6.2. 1. Structural characterization of RIO and degradation products

Table 8. 15- Elemental Composition of RIO and its degradation products

RIO and its DPs	Molecular Formula $[M+H]^+$	Theoretical *m/z*	Experimental *m/z*	Error (ppm)	MS/MS fragment ions
RIO	$C_{20}H_{19}FN_8O_2^+$	423.1649	423.1657	-0.08	391, 109
DP1	$C_{19}H_{17}FN_8^+$	365.1561	365.1607	-0.46	256, 241, 214, 109, 83
DP2	$C_{19}H_{15}FN_8O^+$	391.1323	391.1398	-0.75	149, 109
DP3	$C_{20}H_{19}FN_8O_3^+$	439.1598	439.1612	-0.14	422, 390

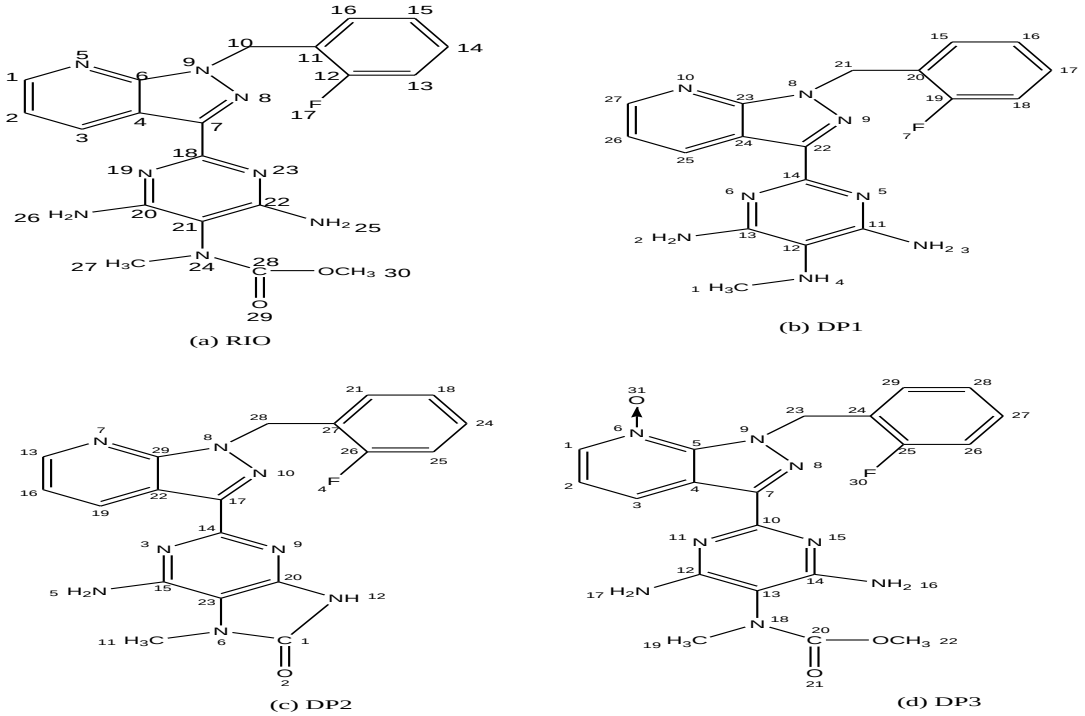

Fig. 8. 26- Structure of RIO and degradation products

8.6.2.1.1. Characterisation of RIO

Mass spectra

An ESI-MS/MS spectrum of RIO is provided in Fig. 8.27 a. ESI-MS/MS spectrum of RIO shows protonated molecular ion peak $[M+H]^+$ at m/z of 423.1659 (Table 8.15) and product ions of m/z 391 (loss of methoxy group from m/z 423), m/z 109(loss of $C_{13}H_{12}N_8O_2$ from *m/z* 423) . Fragmentation pathway of RIO is shown in Fig. 8.27 b.

NMR spectra

^{1}H NMR spectra of RIO shows the presence of methyl group and methoxy group groups at 3.03 and 3.39 ppm. Presence of methylene group is indicated by peak at 5.81 ppm . Methyl and methoxy groups are further confirmed in ^{13}C NMR spectra at 34.72 ppm and 52.51 ppm and methylene group at 43.87 ppm. Two amino groups of pyrimidine ring are indicated in ^{1}H NMR spectra at 6.39 ppm and 6.41 ppm which are absent in D_2O exchange. Protons of pyridine ring are indicated at 9.06, 8.60 and 7.24 ppm. Protons of flurobenzene ring are indicated at 7.12, 7.19 and 7.32 ppm. Presence of ester group in indicated in ^{13}C NMR spectra at 155.52 ppm (Table 8.16).

IR spectra

An IR spectrum of RIO (Fig. 8.31) indicates presence of two primary amino groups at 3508 and 3457 cm^{-1}. Aromatic and methyl groups are merged in the region covering 3099, 3065 and 3035 cm^{-1}.Presence of carbamate functional group is indicated at 1688 cm^{-1} (Table 8.20).

8.6.2.1.2. Characterisation of DP1

Mass spectra

An ESI-MS/MS spectrum of DP1 is provided in Fig. 8.32 a. LC-ESI/MS/MS spectrum of DP1 shows protonated molecular ion peak at m/z of 365.161 with elemental composition $C_{18}H_{17}FN_8^+$ (Table 8.15) shows fragment ions of m/z 256(loss of C_7H_5F group from *m/z* 365), *m/z* 241 (loss of NH from *m/z* 256), *m/z* 214 (loss of C_2H_4N from *m/z* 256), m/z 109 (loss of $C_{11}H_{10}N_8$from *m/z* 365), m/z 83(loss of C_2H_2 from *m/z* 109). Fragmentation pathway of DP1 is shown in Fig. 8.32 b.

NMR spectra

In DP1, there is absence of methyl group and ester group. In ^1H NMR spectra, there are absence of 3 protons which indicates loss of methyl group and other methyl group is shifted towards upfield at 2.51 ppm. There is formation of –NH at 4.00 ppm which is absent in D_2O exchange. ^{13}C NMR spectra of DP1 indicates absence of ester functional group at 155 ppm, absence of one methyl group at 52.52 ppm (Table 8.17).

IR spectra

An IR spectrum of DP1 indicates presence of primary amino group at 3463 cm^{-1} and secondary amino group at 3329 cm-1. Presence of aromatic group is indicated at 3266 and 3125 cm^{-1}. There is absence of ester group at 1688 cm^{-1} which is present in RIO (Table 8.20) (Fig. 8.36).

Mechanism of formation of DP1

DP1 is formed from RIO by bimolecular elimination reaction. In alkaline hydrolysis there is nucleophilic attack of hydroxide ion on carbonyl group of carbamate, there is formation of tetrahedral intermediate. Tetrahedral intermediate loses methoxy group, carboxylic acid intermediate is formed. Carboxylic acid intermediate loses carbon dioxide and DP1 is formed (Fig. 8.32 c).

Based on the above DP1 is characterised as 2-(1-(2-fluorobenzyl)-1H-pyrazolo[3,4-b]pyridin-3yl)-N5-methylpyrimidine-4,5,6-triamine.

8.6.2.1.3. Characterisation of DP2

Mass spectra

ESI-MS/MS spectrum of DP2 is provided in Fig. 8.37 a. LC-ESI-MS/MS spectrum of DP2 shows protonated molecular ion at m/z 391.1396 with elemental composition $C_{19}H_{15}FN_8O^+$ (Table 8.15). DP2 shows fragment ions of *m/z* 149 (loss of $C_{14}H_{12}FN_3$ group from *m/z* 391), m/z 109 (loss of $C_{11}H_{10}N_8$ from m/z 391). Fragmentation pathway of DP2 is shown in Fig. 8.37b.

NMR spectra

^{1}H NMR spectra shows absence of one of the methyl protons, there is formation of –NH(-NHCO) at 11.6 ppm. There is loss of ester group and formation of imidazolinone at 152.52 ppm, loss of one of the methyl group is indicated by at absence of peak 52.52 ppm (Table 8.18).

IR spectra

IR spectra of DP2 (Fig. 8.41) indicates presence of primary and secondary amine at 3515 and 3282 cm^{-1}. Formation of carbonyl group is indicated by formation of peak at 1710 cm^{-1} (Table 8.20).

Mechanism of formation of DP2

DP2 is formed from RIO in alkaline condition. In the first step there is elimination of methyl group from carbamate. Lone pair of electrons of amino group of pyrimidine ring attack on carbonyl carbon, intermediate is formed. Loss of proton from intermediate causes formation of DP2 (Fig.8.37c).

Based on the above, DP2 is characterised as 2-(1-(2-fluorobenzyl)-1H-pyrazolo[3,4-b]pyridin-3-yl)-6-amino-7-methyl-7H-purin-8(9H)-one.

8.6.2.3.4. Characterisation of DP3

Mass spectra

An ESI-MS/MS spectrum of DP3 is provided in Fig. 8.42 a. LC-ESI/MS/MS spectra of DP3 shows protonated molecular ion at 439.1612 with elemental composition of $C_{20}H_{19}FN_8O_3^+$ (Table 8.15). DP3 shows fragment ions of m/z 422 (loss of methane from m/z 439), m/z 390 (loss of methanol from m/z 422). Fragmentation pathway of DP3 is shown in Fig. 8.42 b.

NMR spectra

The number of protons and number of carbons in DP3 are same as in ^{1}H and ^{13}C NMR spectra as that of RIO. In the protons of pyridine ring chemical shift is observed in three protons compared to RIO which indicates that formation of N-oxide has taken place in pyridine ring and there is chemical shift value in these protons (Table 8.19).

IR spectra

IR spectra of DP3 (Fig. 8.49) indicates broad peak in region 3371, 3261, 3010 cm^{-1} indicating the presence of primary, secondary amine, aromatic group and N-oxide. Presence of ester group is indicated at 1703 cm^{-1} (Table 8.20).

Mechanism of formation of DP3

DP3 may be formed from RIO by oxidation. Hydrogen peroxide gets broken to hydroxide ion. There is attack of hydroxide ion on pyridine nucleus of RIO which results in formation of N-hydroxide, from which proton is lost and there is formation of N-oxide of RIO, degradation product DP3 (Fig. 8.42 c).

Based on the above DP3 is characterized as methyl 2-(1-(2-fluorobenzyl)-1H-pyrazolo [3, 4-b] pyridin-3-yl)-4, 6-diaminopyrimidin-5-ylmethylcarbamate-N-oxide.

Table 8. 16- NMR assignments of RIO

RIO				
Position	**^{1}H (Fig. 8.28)**	**Chemical Shift(δ ppm)**	**Position**	**^{13} C (Fig. 8.29) and APT* (Fig. 8.30)**

1,2,3	3H	9.06(d),8.60(d), 7.24(d)	22	158.60 Quaternary Carbon
13,14, 15,16	4H	7.12(d),7.31(m),7.19 (d),7.31(m)	28	155.52 Ester
25, 26	4H	6.39,s, 6.41, s absent in D_2O exchange	1, 2, 3	148.89,117.89,133.82 Aromatic -CH-
10	2H	5.81, s	4, 6	114.65, 155.09 Quaternary Carbon
27	3H	3.03,s	7	141.78 Quaternary Carbon
30	3H	3.39,s	11, 12	124.24, 161.04, Quaternary Carbon
			13,14,15, 16	115.52,129.74,124.53, 129.83Aromatic -CH-
			18,20,21	150.78, 159.50, 100.27, 158.60 Quaternary Carbon
			30	52.51, CH_3
			10	43.87,CH_2
			27	34.72,CH_3

*CH_3 and CH as positive peaks, CH_2 and quaternary carbon as negative peaks

Table 8. 17- NMR assignments of DP1

DP1				
Position	**^{1}H (Fig. 8.33)**	**Chemical Shift (δ ppm)**	**Position**	**^{13}C (Fig.8.34) and APT (Fig. 8.35)**
25,26,27	3H	7.35(d),8.6(d),9.06(d)	22, 23,24	142.08, 153.09, 114.49 Quaternary carbon

15,16,17,18	4H	7.35(d),7.13(d), 7.31 (t),7.12(d)	25,26, 27	133.82, 115.52,148.8 Aromatic-CH-
2	2H	6.09,s, absent in D_2O exchange	15,16,17,18	129.92,124.52, 129.81, 115.31 Aromatic –CH-
3	2H	6.09,s, absent in D_2Oexchange	19,20	161.05,124.56 Quaternary carbon
21	2H	5.79,s	11,12,13, 14	158.61,106.98, 158.26, 150.78 Quaternary carbon
4	1H	3.39,s-NH,absent in D_2O exchange	21	43.75,CH_2
1	3H	2.51,d	1	33.06,CH_3

Table 8. 18- NMR assignments of DP2

DP2				
Position	**^{1}H(Fig. 8.38)**	**Chemical Shift (δ ppm)**	**Position**	**^{13}C (Fig. 8.39) and APT (Fig. 8.40)**
12	1H	11.6, -NH absent in D_2O exchange	1	152.52, imidazolinone
13, 16, 19	3H	9.06(d), 8.63(d), 7.37 (d)	13,16,19	149.06, 117.98, 133.37 Aromatic-CH-
18,21,24,25	4H	7.22 (d), 7.35(d), 7.24(d), 7.20 (d)	22, 29,17	114.27,152.92,141.39 ,Quaternary carbon
5	2H	6.76, s, -NH_2 absent in D_2O exchange	18,21, 24	124.56,130.16,129.91,Aromatic –CH-
28	2H	5.80,s	25,26,27	115.55,161.33,124.59,

				Quaternary carbon
11	3H	3.49,d	14,15,20, 23	150.78, 158.68, 147.8,105.19, Quaternary carbon
			28	43.87 CH_3
			11	28.27 CH_3

Table 8. 19- NMR assignments of DP3

DP3				
Position	**^{1}H (Fig. 8.43)**	**Chemical Shift (δ ppm)**	**Position**	**^{13}C (Fig. 8.44) and APT (Fig. 8.45)**
1,2,3	3H	8.65(d), 7.41(s), 8.54 (d)	1,2,3	149.06, 117.47, 134.34 Aromatic –CH-
26,27,28,29	4H	7.18 (d), 7.27(d), 7.23(d), 7.31(d)	4,5,7	114.86, 152.86, 137.25 Quaternary carbon
17	2H	7.2,s,-NH_2 absent in D_2O exchange	10,12,13,14	140.09,158.66, 99.96, 158.76 Quaternary carbon
16	2H	6.8,s, ,-NH_2 absent in D_2O exchange	24,25,26,27,28,29	124.62, 161.10, 115.59,129.96,123.87,130.21 Aromatic –CH-
23	2H	5.81, s	20	154.99 Ester
19	3H	3.49,3.46,d	22	52.61 CH_3
22	3H	2.90,s	23	43.94 CH_2
			19	34.54 CH_3

Table 8. 20- IR interpretation of RIO, DP1, DP2 and DP3

RIO		DP1		DP2		DP3	
Wave number (cm^{-1})	Assignments	Wave number (cm^{-1})	Assignments	Wave number (cm^{-1})	Assignments	Wave number (cm^{-1})	Assignments
3508,3457	N-H (Stretching)	3463,3329	N-H (Stretching)	3515, 3282,	N-H Stretching	3371, 3261 3010	Broad peak covering –N-H, Aromatic C-H Stretching and N-oxide
3099, 3064,3035	Aromatic C-H and Methyl C-H stretching			3153	Aromatic C-H Stretching		
		3266, 3125	Aromatic C-H Stretching	2988, 2967	Methyl C-H Stretching	2747	Methyl C-H Stretching
						1703	Ester C=O Stretching
1688	C=O Stretching	1598, 1568,1459	Aromatic C=C Bending	1711	Carbonyl C=O Stretching	1636	Aromatic C-H bending
1622	Aromatic C=C Stretching			1639	Aromatic C=C stretching	1633	
1602				1602		1522	
1505				1596			

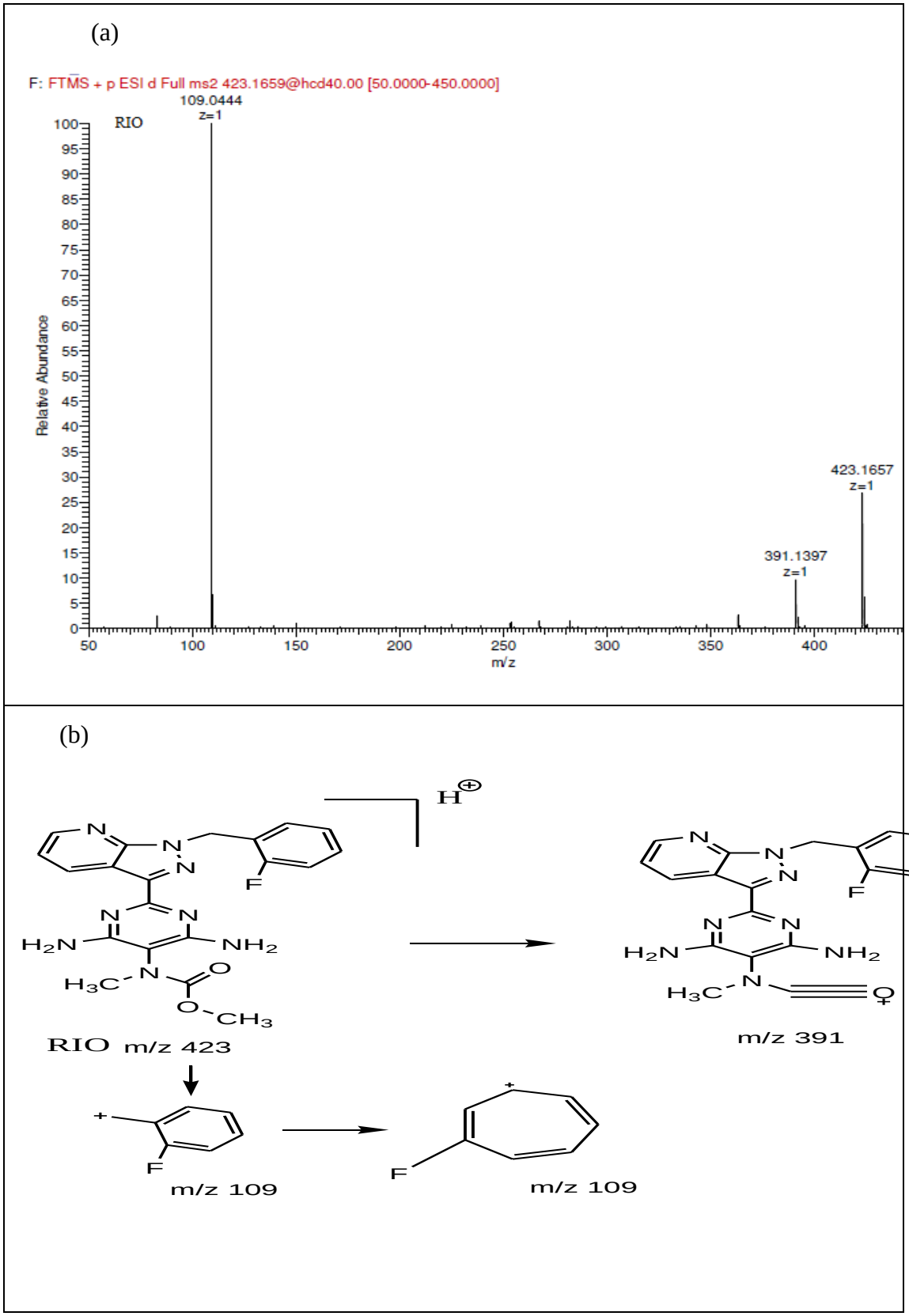

Fig. 8. 27-(a) ESI-MS/MS spectra (b) Fragmentation pathway of RIO

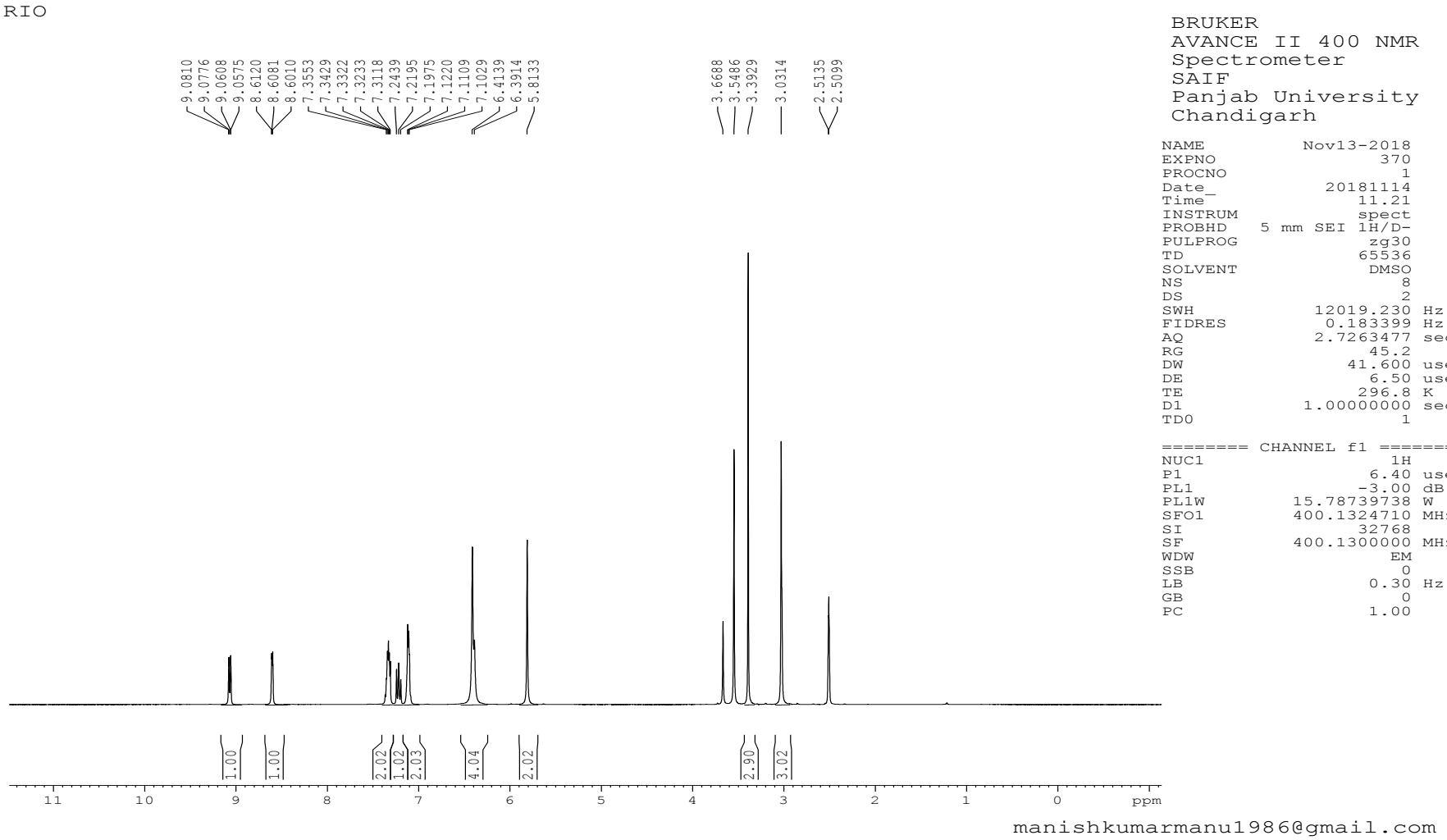

Fig. 8. 28- ^{1}H NMR spectra of RIO

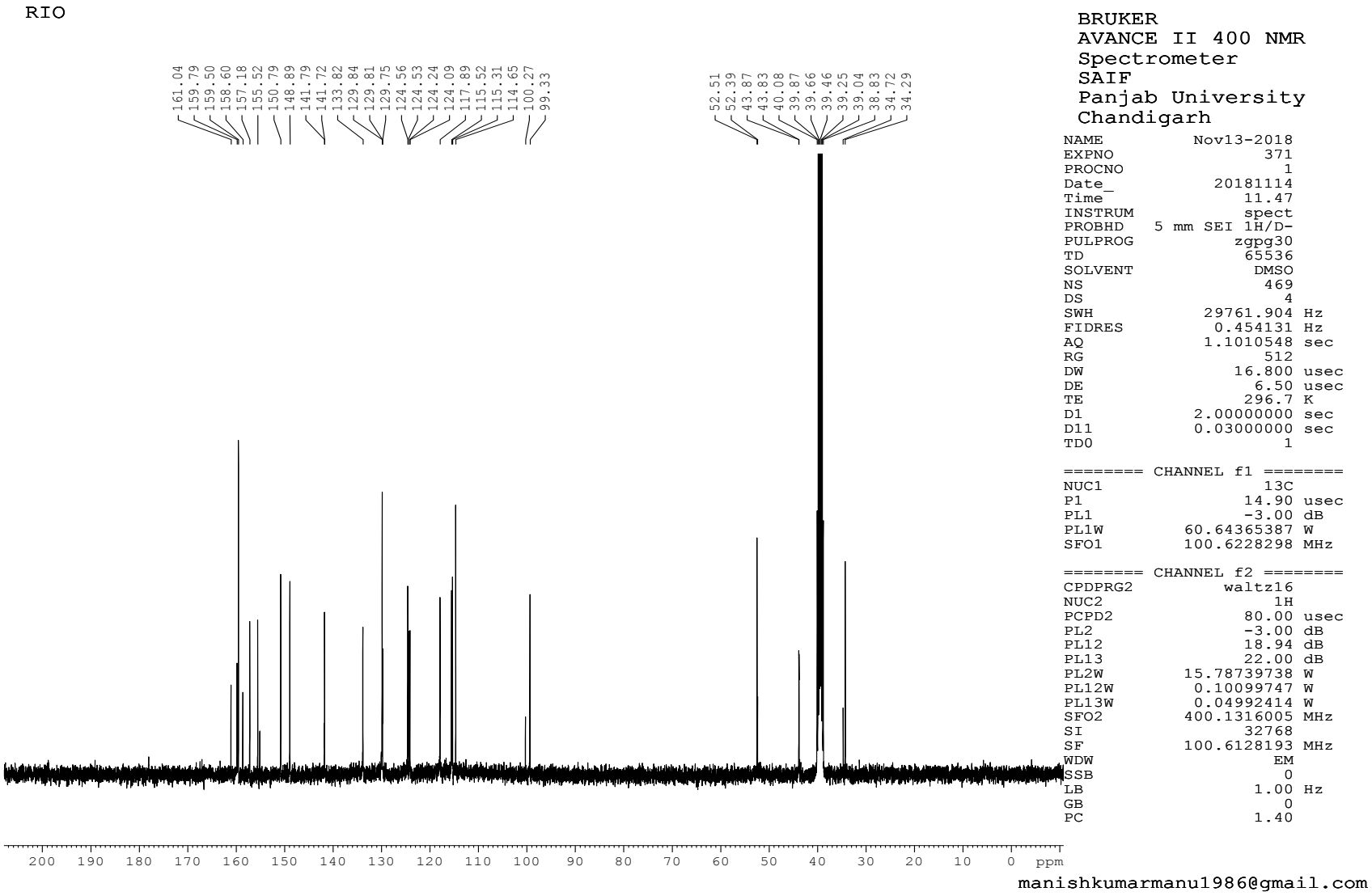

Fig. 8. 29- ^{13}C NMR spectra of RIO

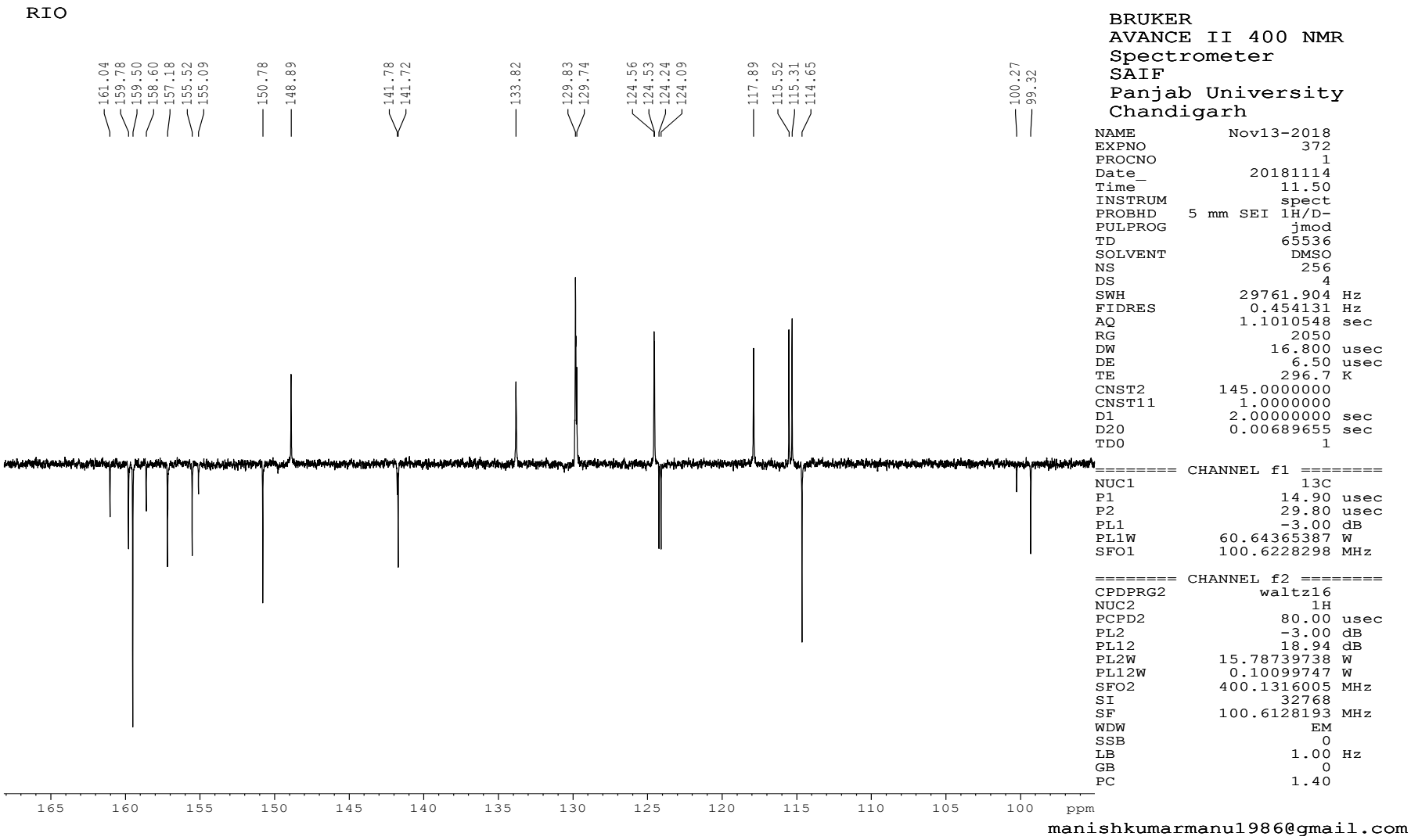

Fig. 8. 30- APT spectra of RIO

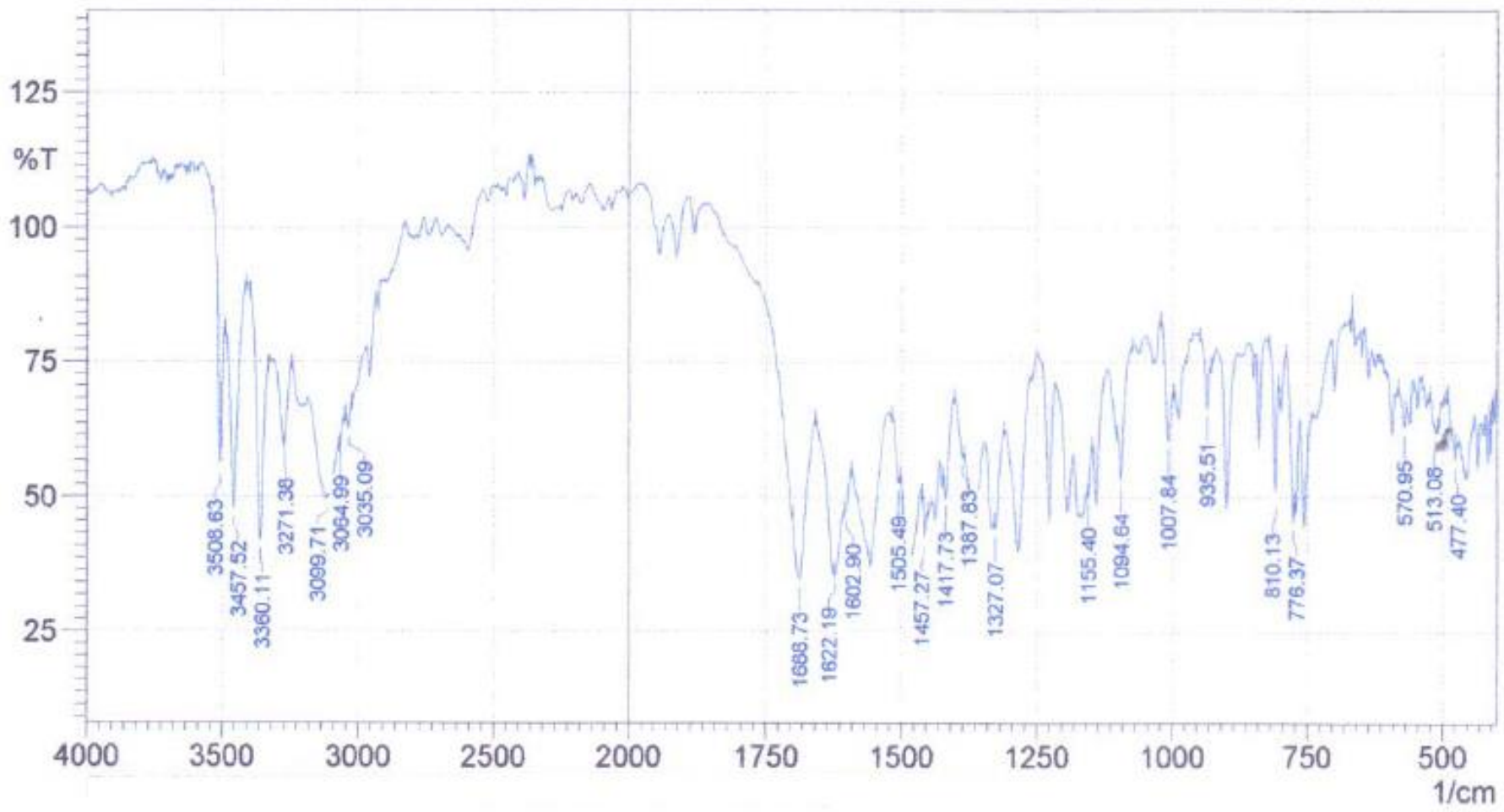

Fig. 8. 31- IR spectra of RIO

(a)

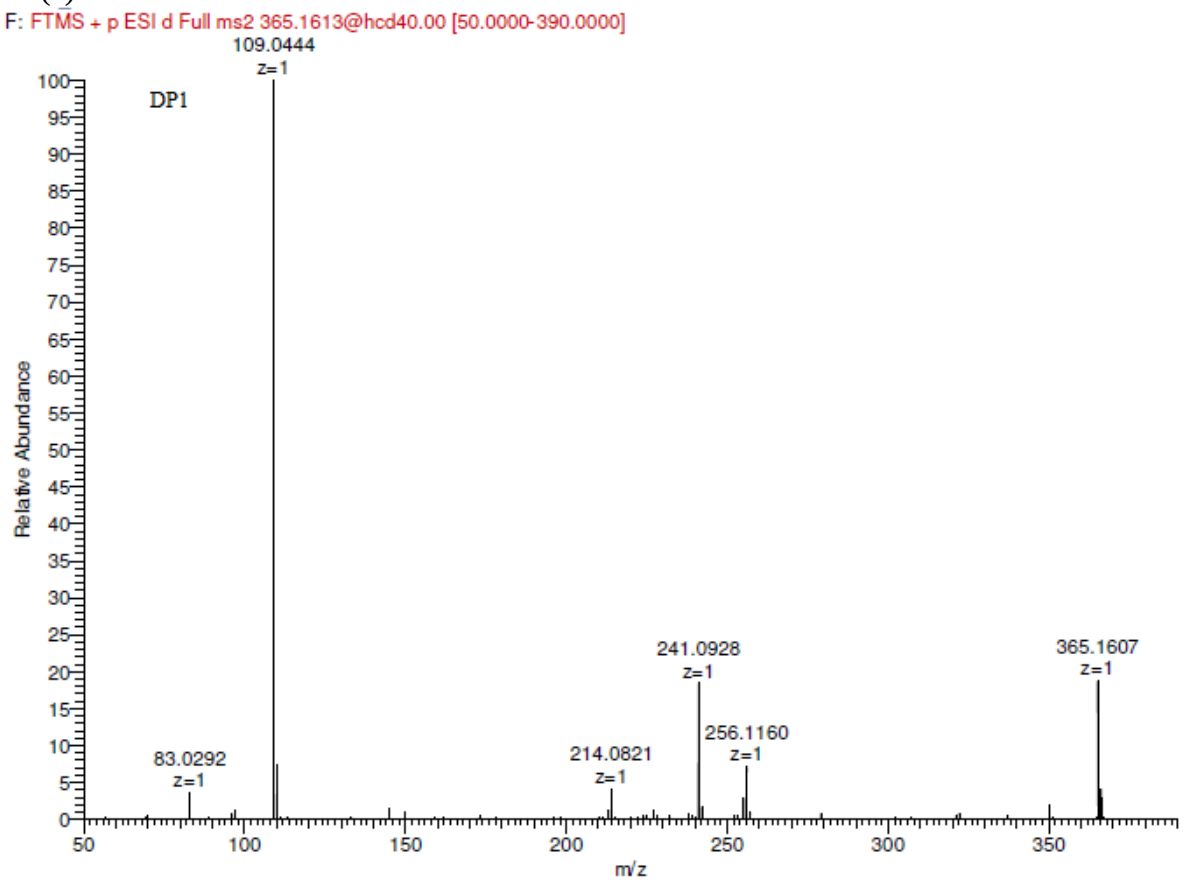
F: FTMS + p ESI d Full ms2 365.1613@hcd40.00 [50.0000-390.0000]
109.0444
z=1
DP1
Relative Abundance
m/z
83.0292
z=1
214.0821
z=1
241.0928
z=1
256.1160
z=1
365.1607
z=1

(b)

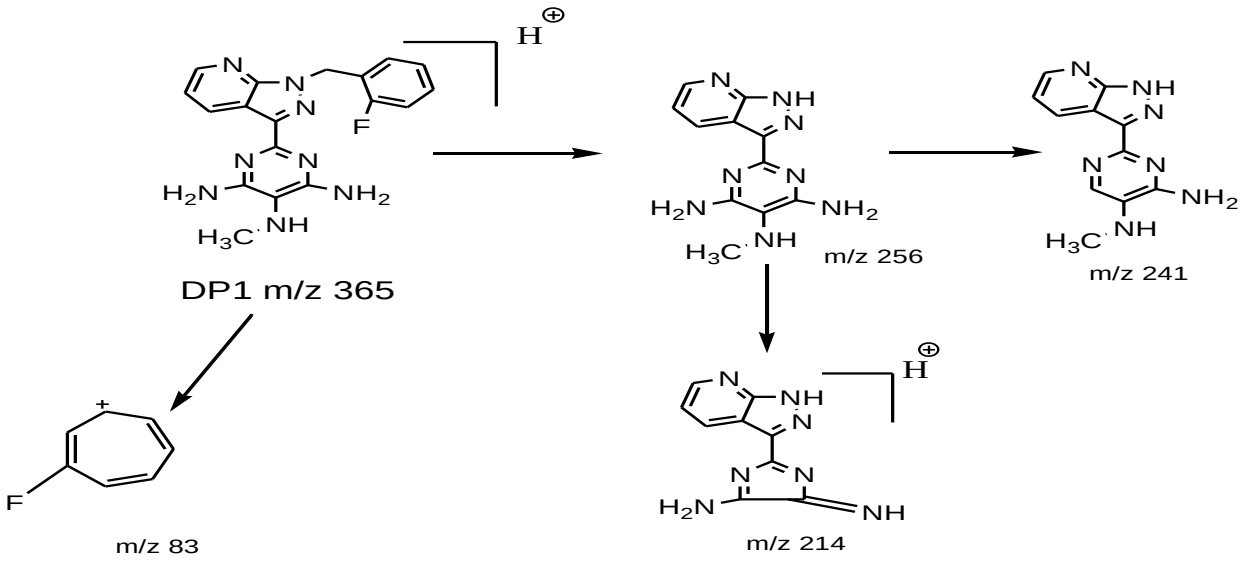
DP1 m/z 365
m/z 83
m/z 256
m/z 241
m/z 214

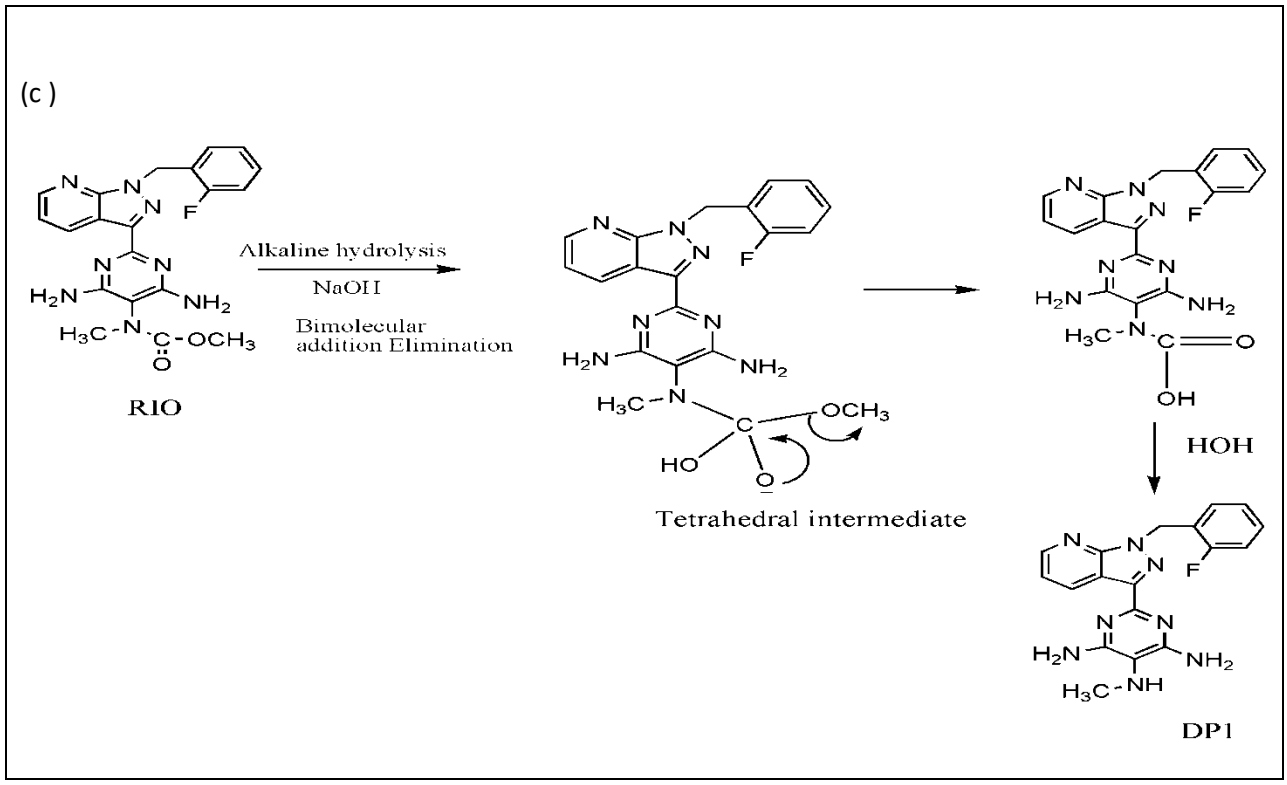

Fig. 8. 32- (a) ESI-MS/MS spectra (b) Fragmentation pathway of DP1 (c) Mechanism of DP1

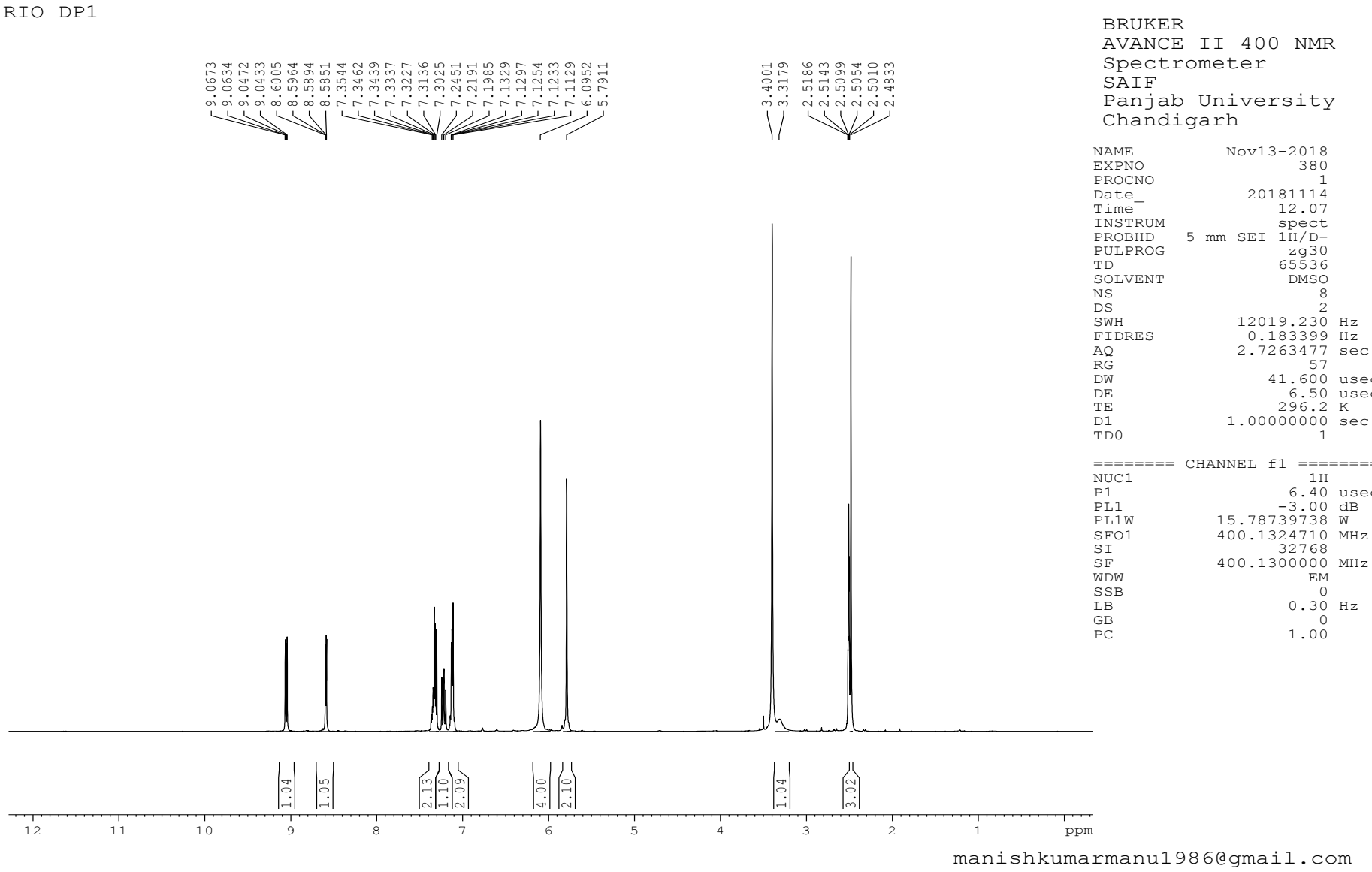

Fig. 8. 33- ^{1}H NMR spectra of DP1

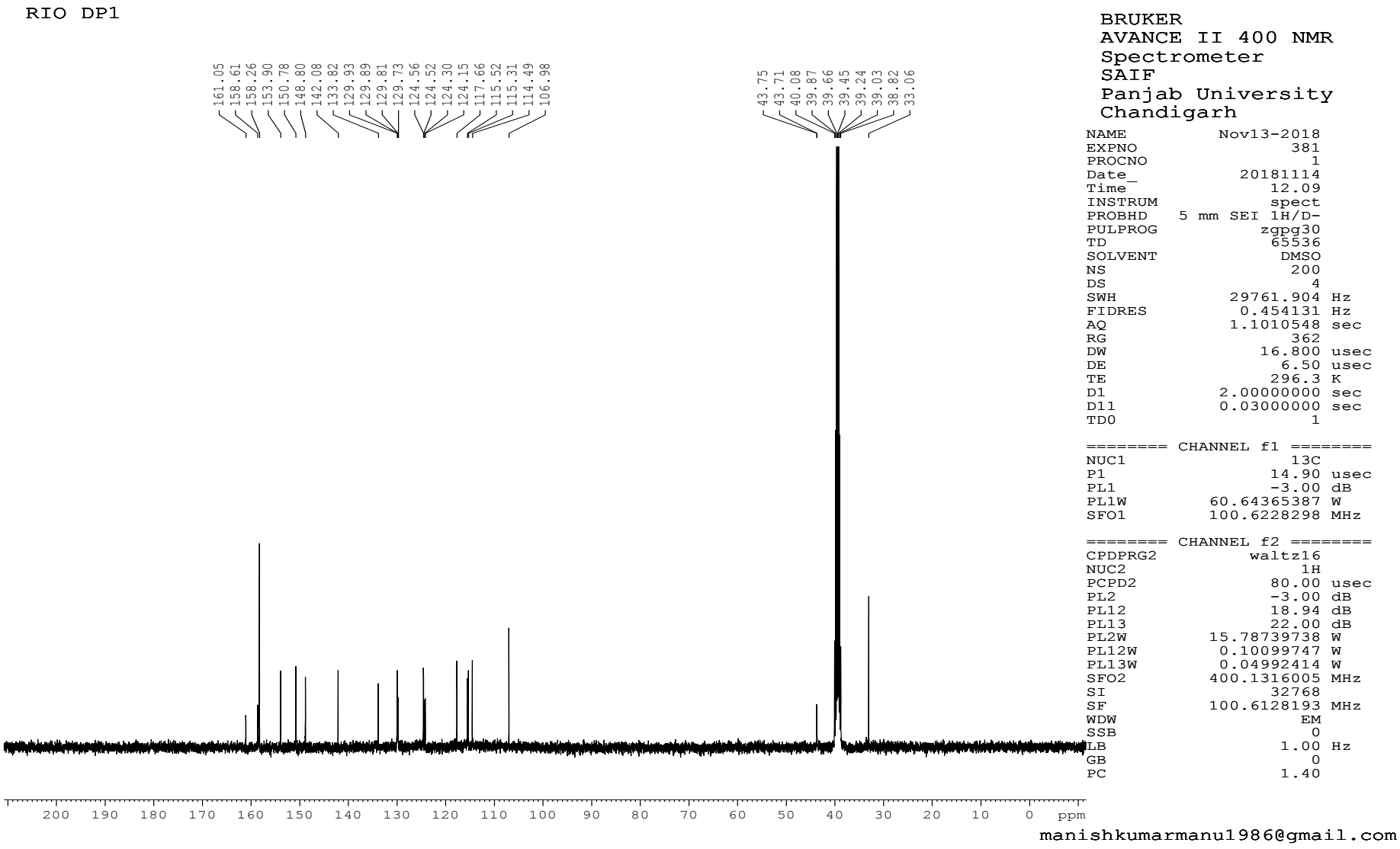

Fig. 8. 34- ^{13}C NMR spectra of DP1

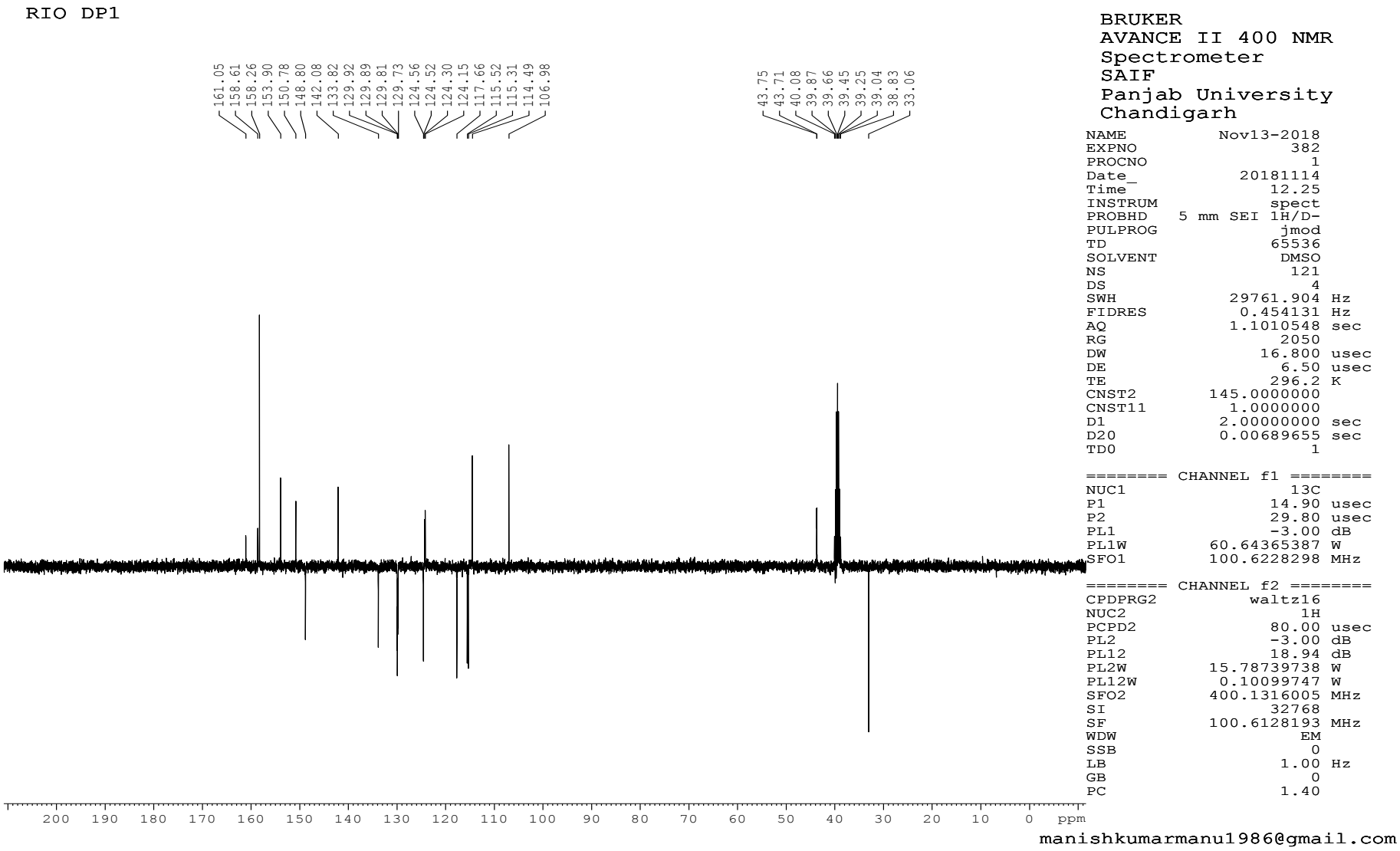

Fig. 8. 35- APT spectra of DP1

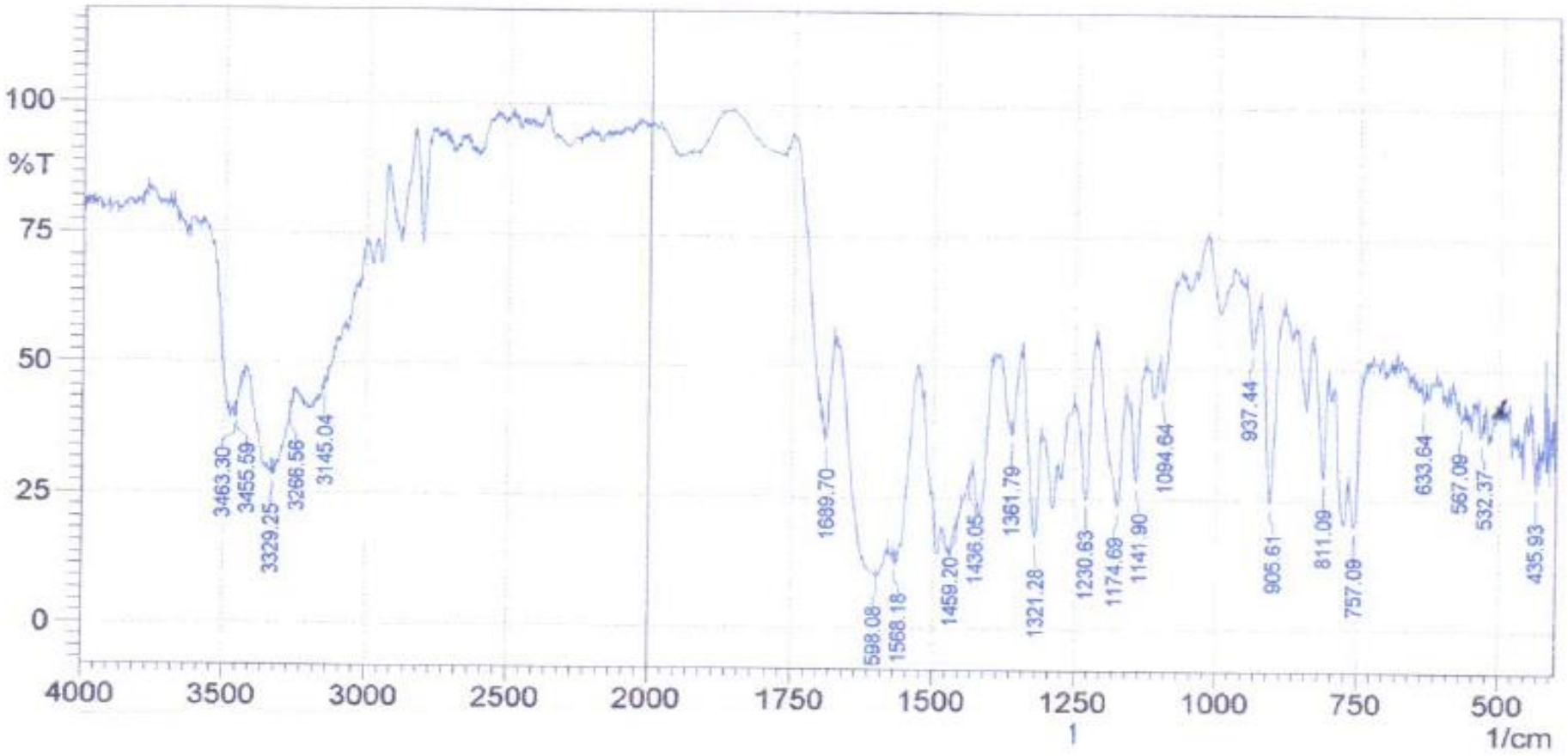

Fig. 8. 36- IR spectra of DP1

(a)

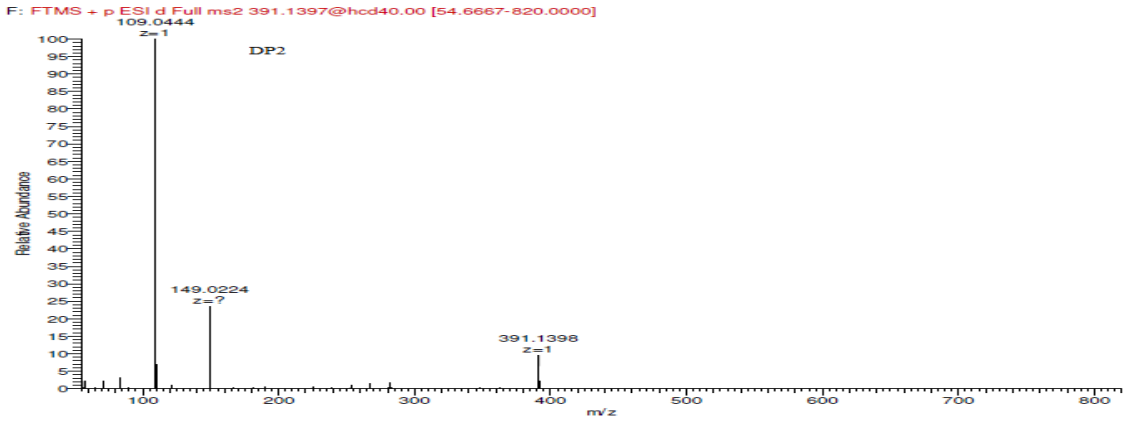
F: FTMS + p ESI d Full ms2 391.1397@hcd40.00 [54.6667-820.0000]
109.0444
z=1
DP2
149.0224
z=?
391.1398
z=1
Relative Abundance
m/z

(b)

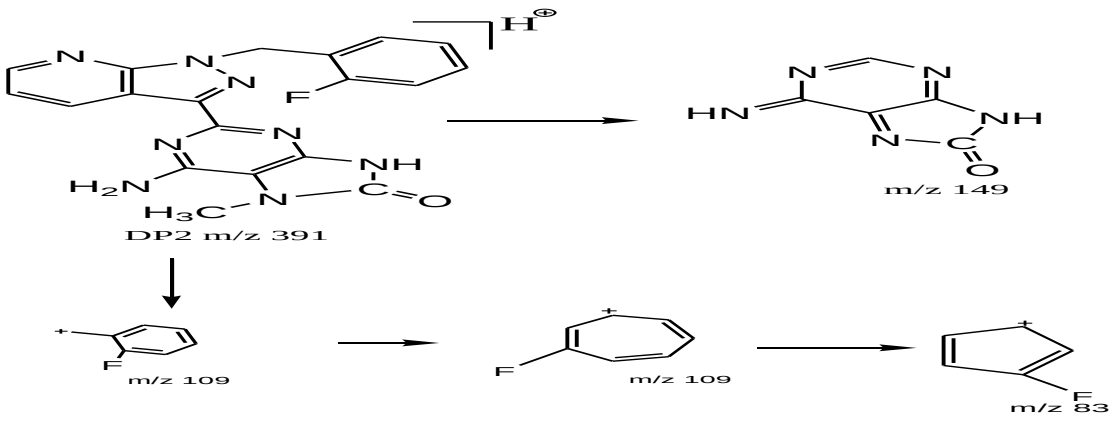
DP2 m/z 391
m/z 149
m/z 109
m/z 109
m/z 83

(c)

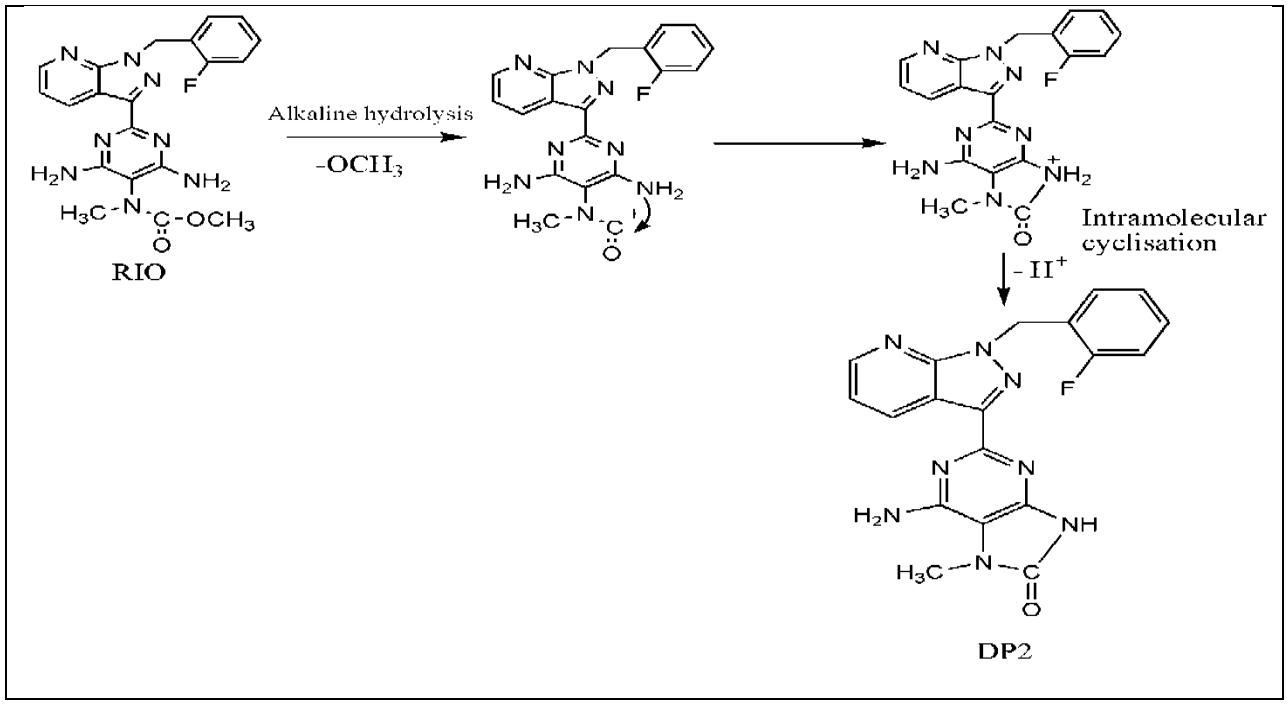

Fig. 8. 37- (a) ESI-MS/MS spectra (b) Fragmentation pathway (c) Mechanism of formationDP2

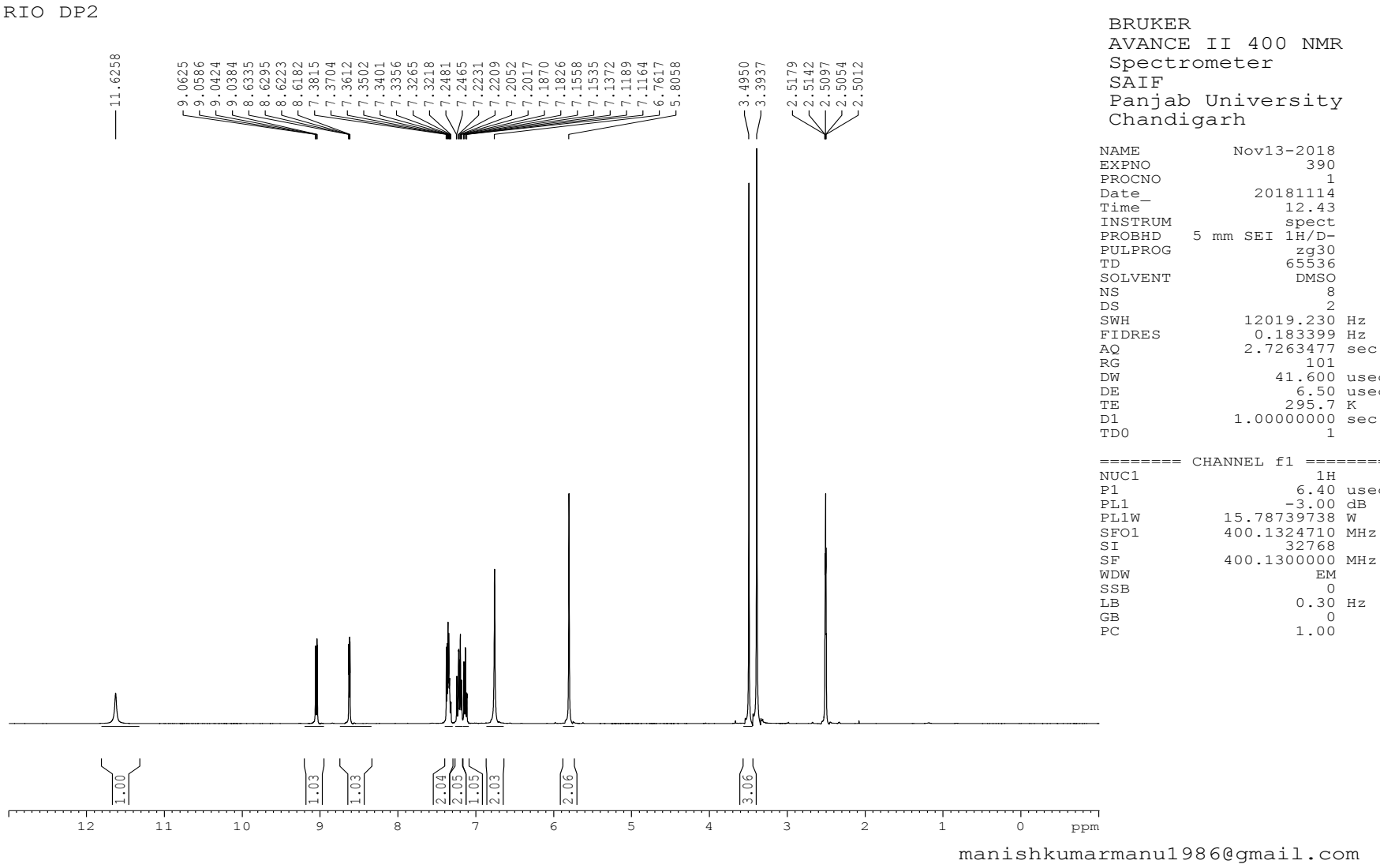

Fig. 8. 38- ^{1}H NMR spectra of DP2

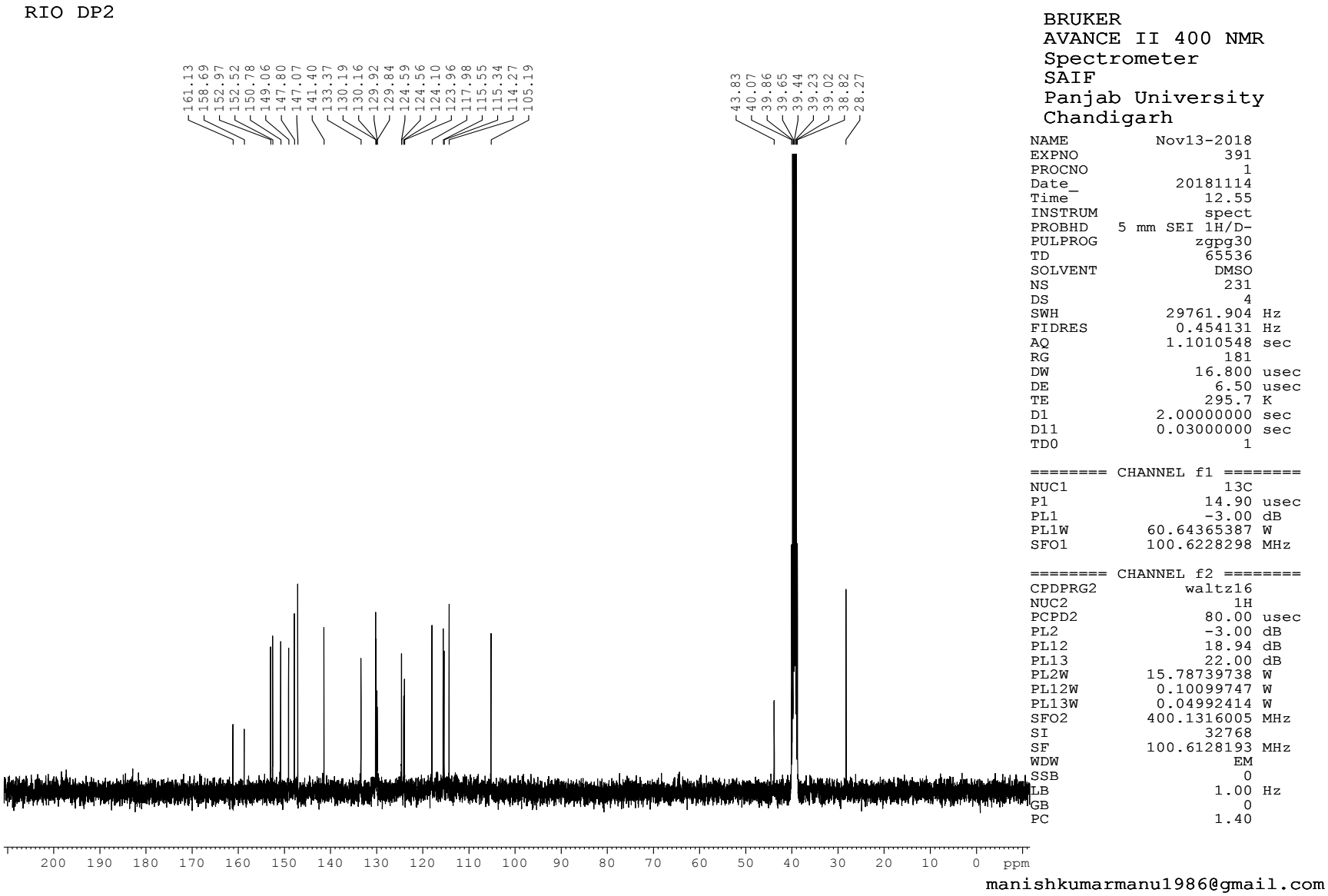

Fig. 8. 39- ^{13}C NMR spectra of DP2

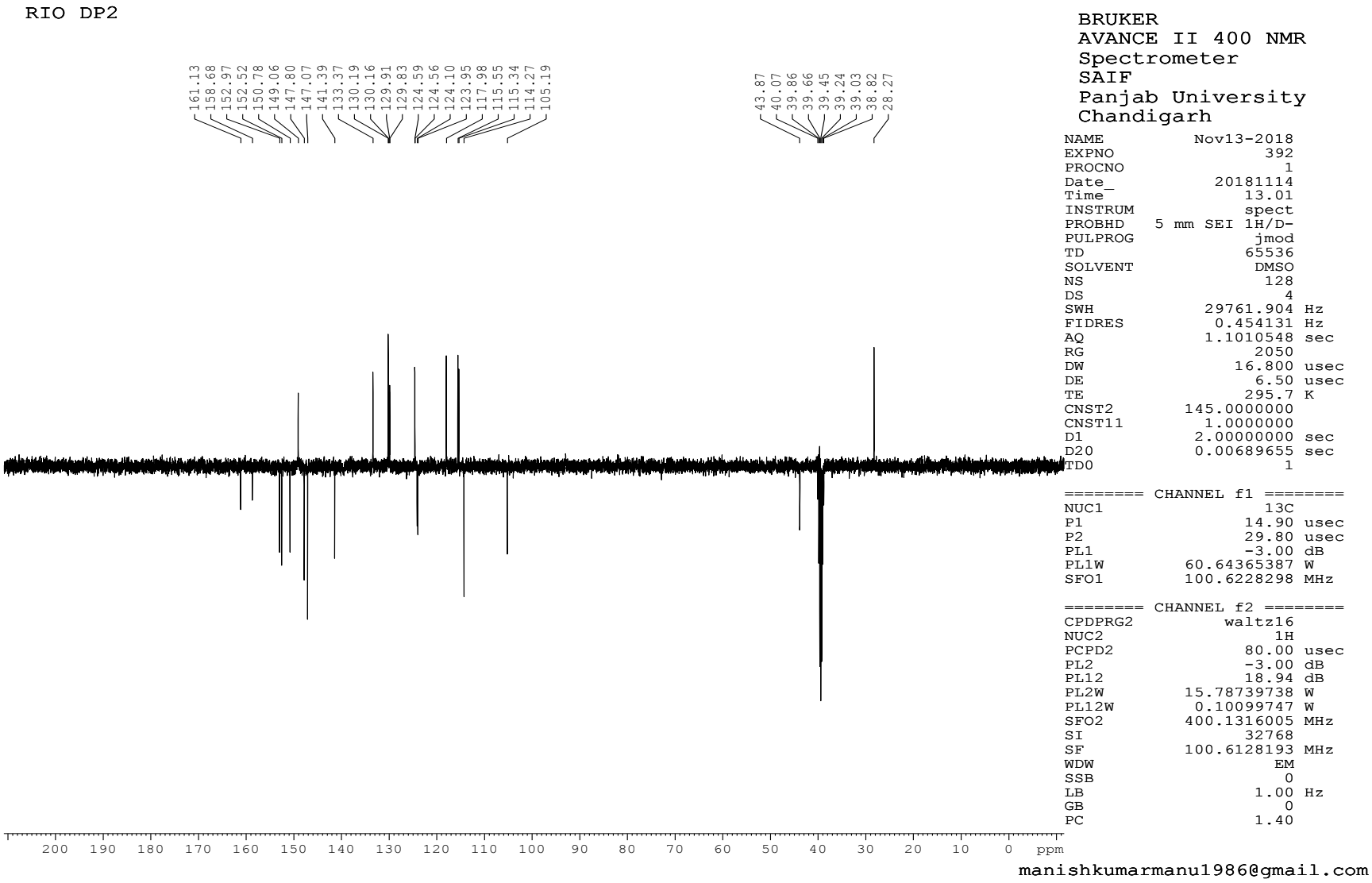

Fig. 8. 40- APT spectra of DP2

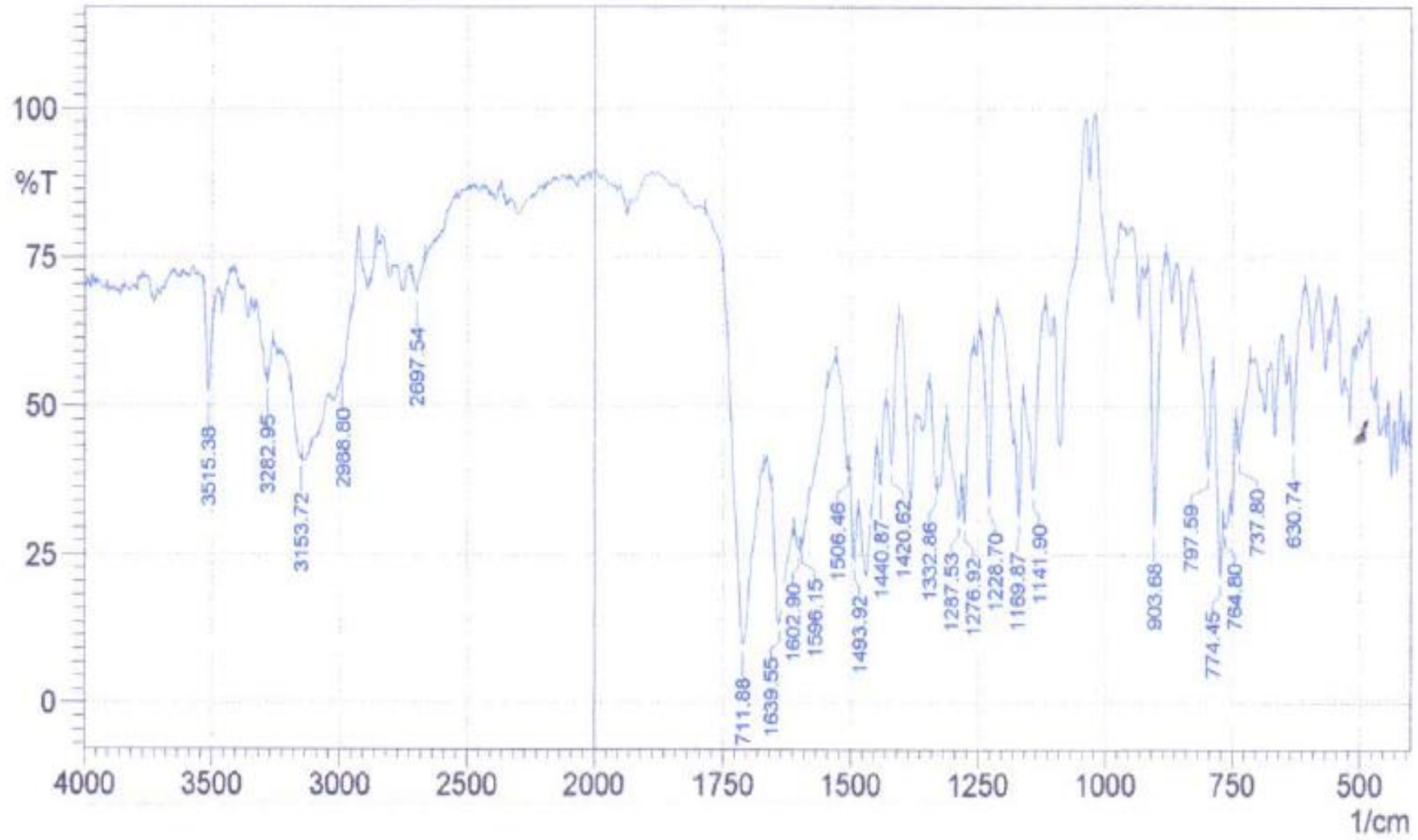

Fig. 8. 41 - IR spectra of DP2

(a)

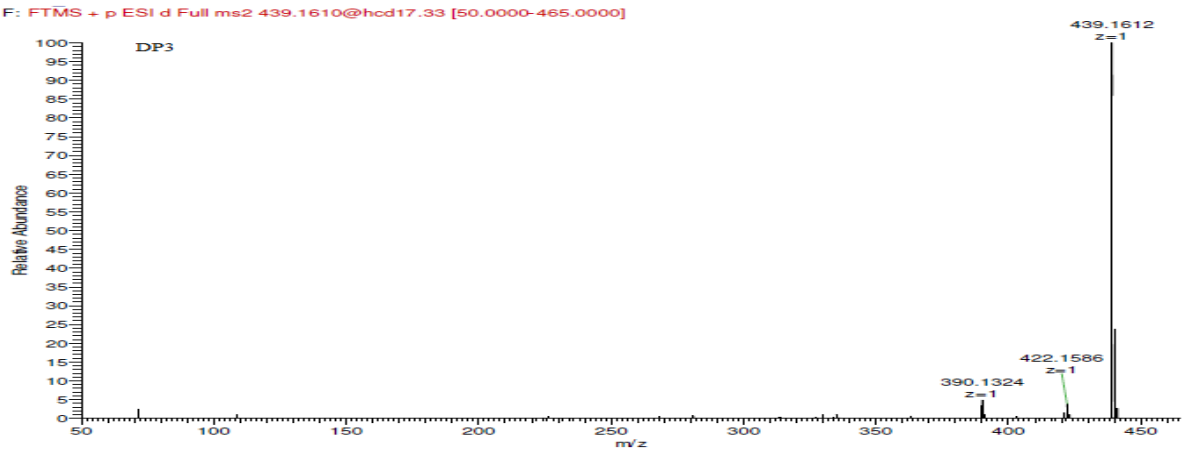
F: FTMS + p ESI d Full ms2 439.1610@hcd17.33 [50.0000-465.0000]
DP3
439.1612
z=1
422.1586
z=1
390.1324
z=1
Relative Abundance
m/z

(b)

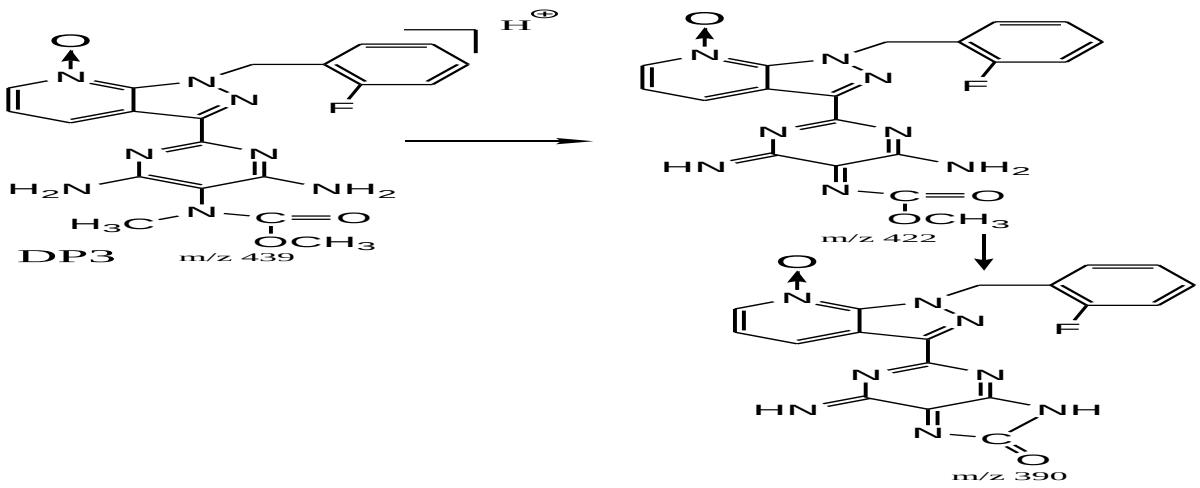
DP3
m/z 439
m/z 422
m/z 390

(c)

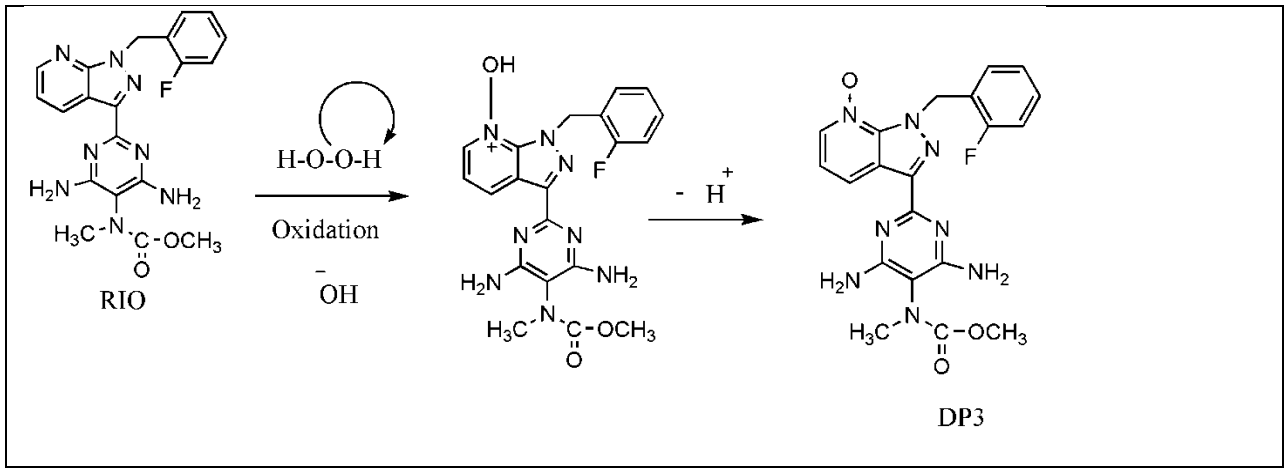

Fig. 8. 42-(a) ESI-MS/MS spectra (b) Fragmentation pathway (c) Mechanism of formation of DP3

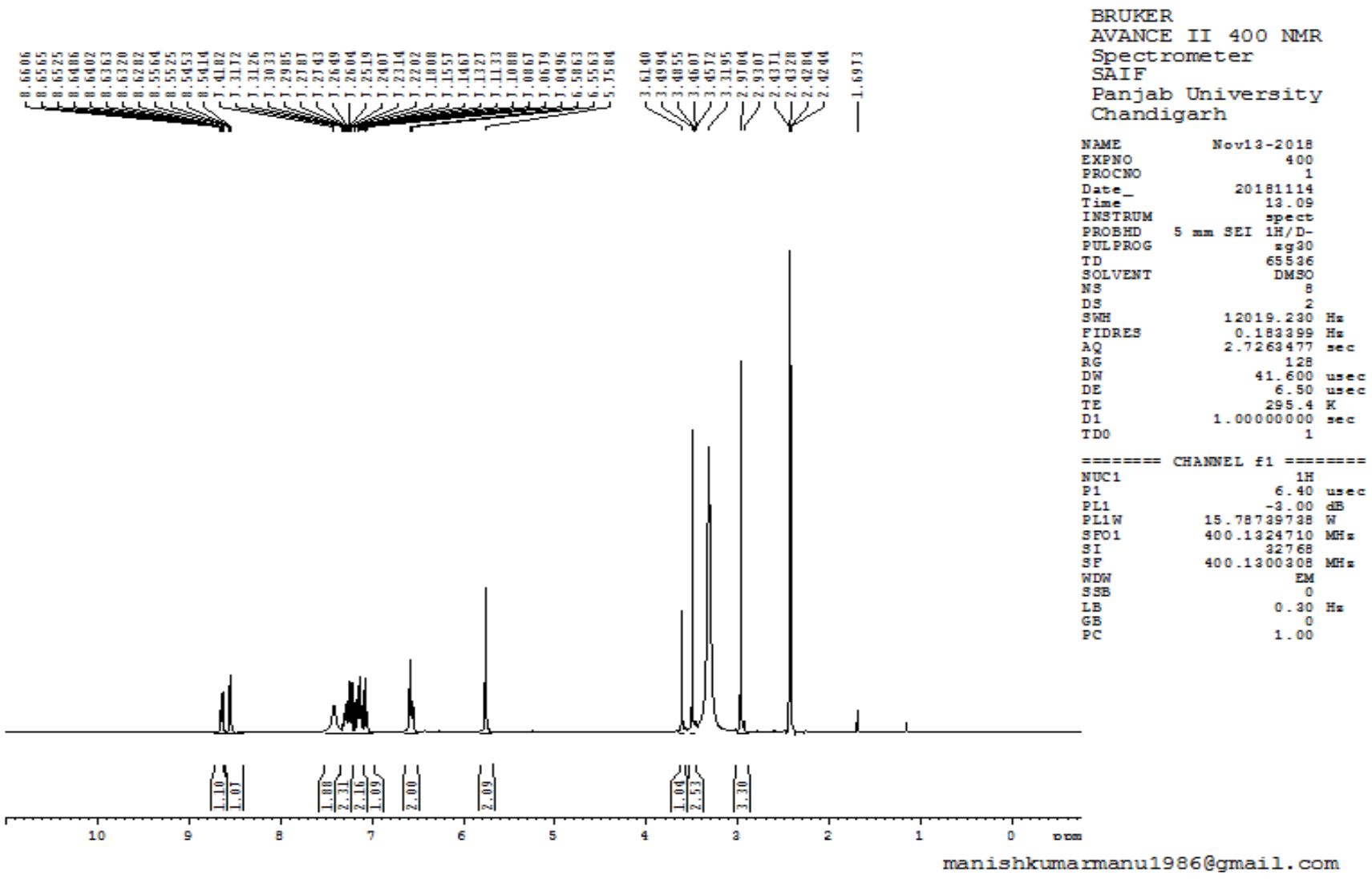

Fig. 8. 43- ^{1}H NMR spectra of DP3

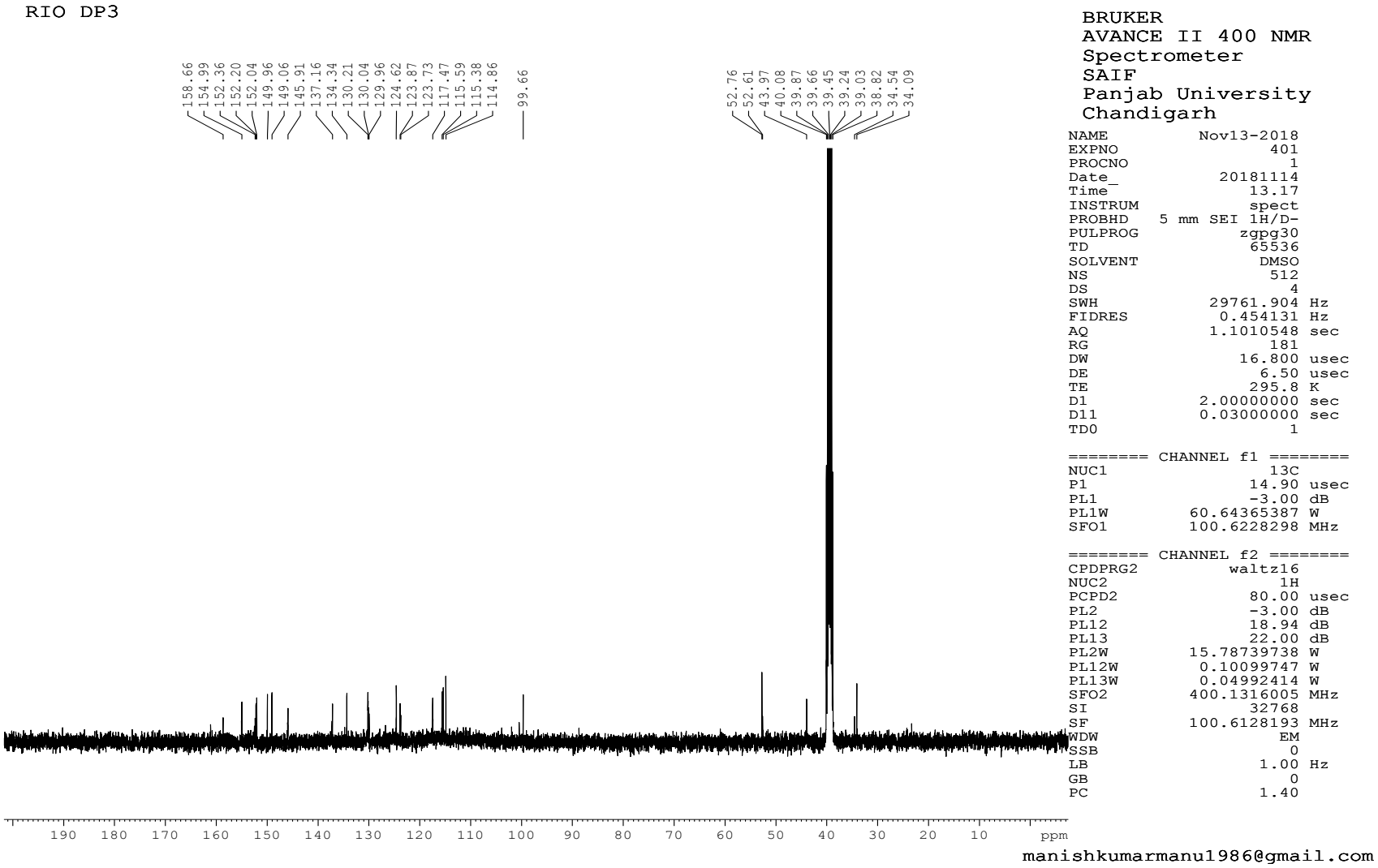

Fig. 8. 44- ^{13}C NMR spectra of DP3

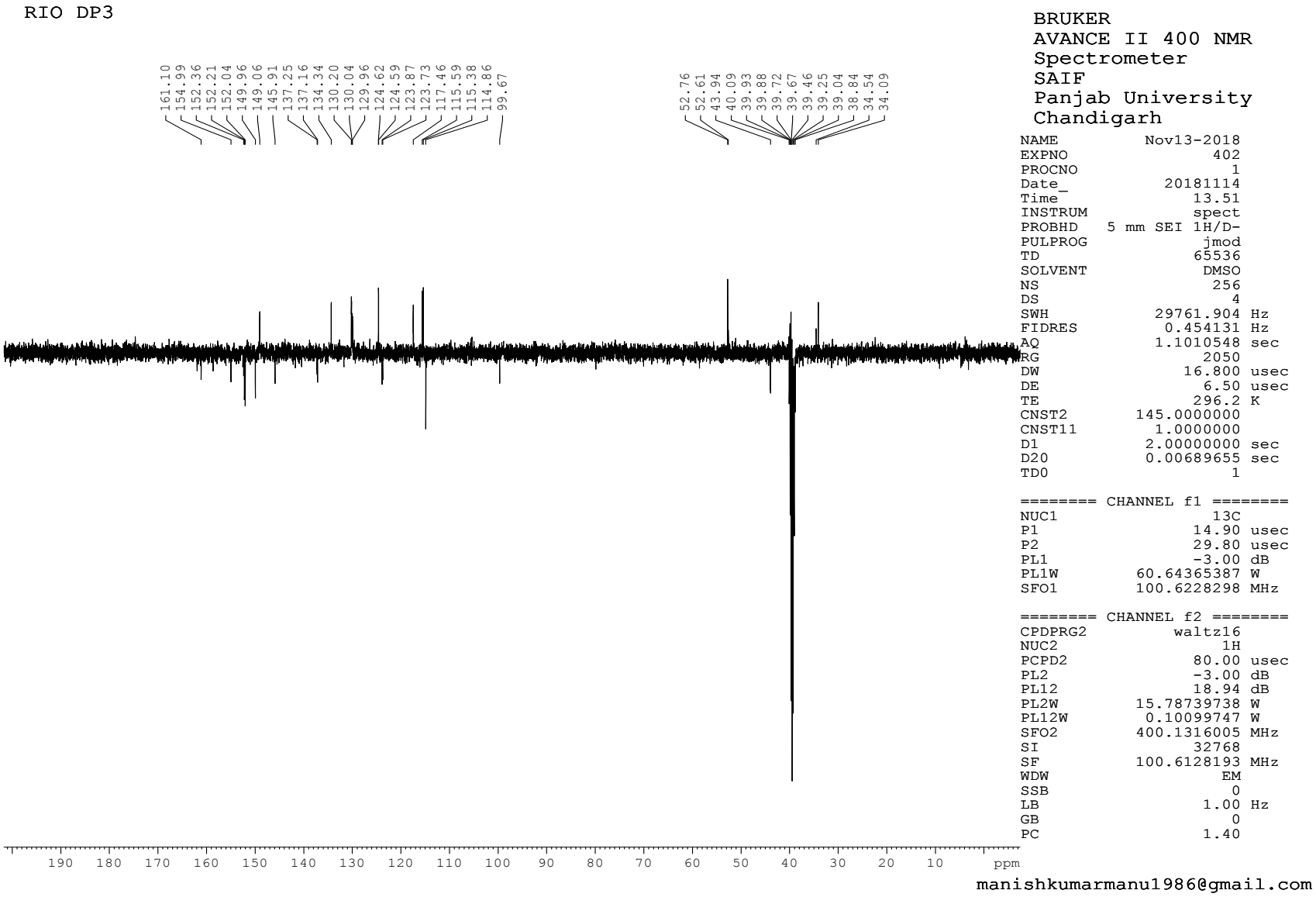

Fig. 8. 45- APT spectra of DP3

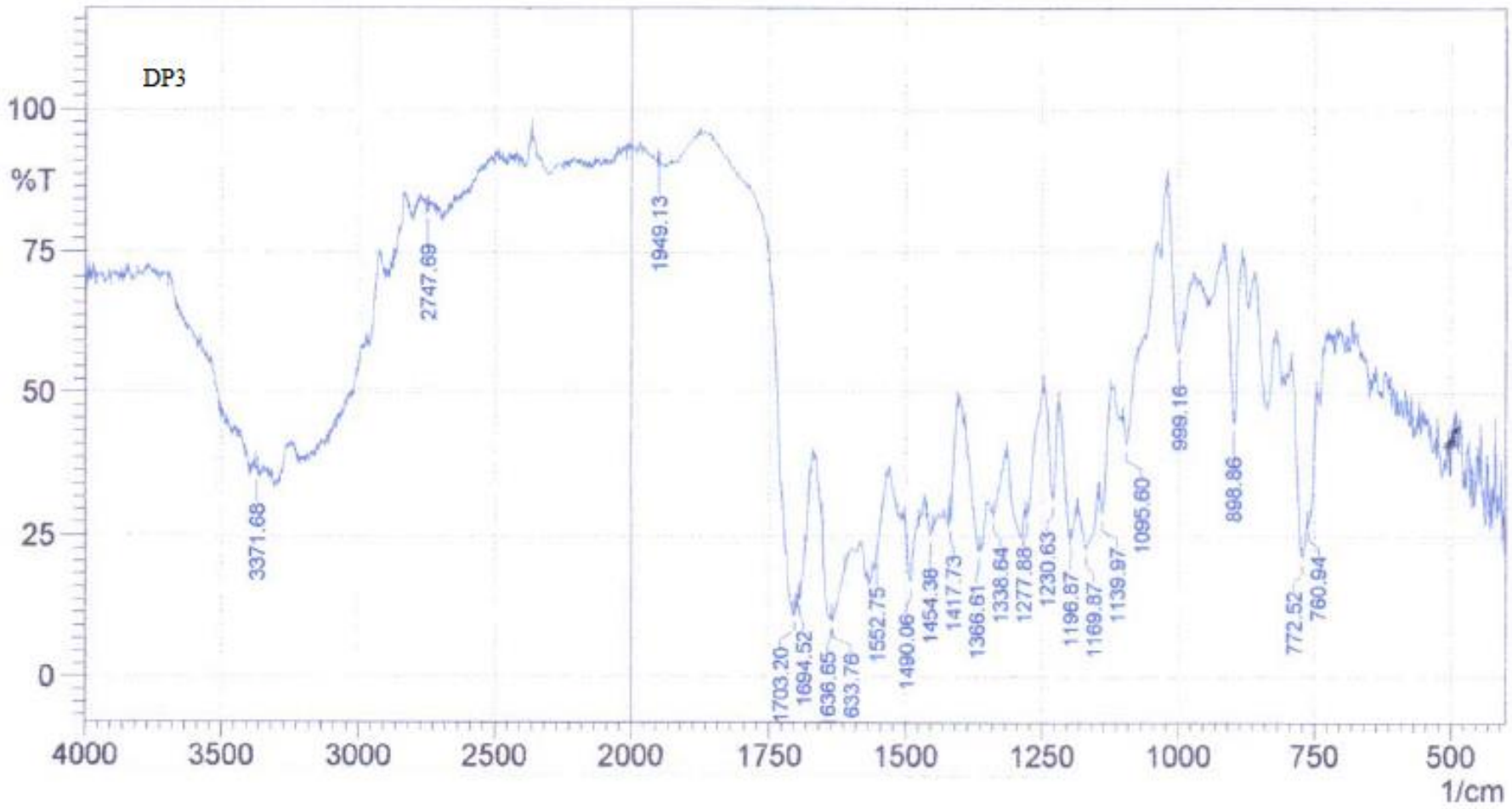

Fig. 8. 46- IR spectra of DP3

8.6.3. DISCUSSIONS

Major degradation product DP1, DP2 in alkaline and DP3 in oxidative condition were isolated and purified by preparative HPLC.

Mass spectra of DP1 shows protonated molecular ion peak at m/z of 365.161.DP1 has 58 amu less than RIO which may be due to loss of methyl group and carbamate functional group. In ^{1}H NMR spectra there are absence of 3 protons which indicates loss of methyl group other methyl group is shifted towards upfield at 2.51 ppm. There is formation of –NH at 4.00 ppm which is absent in D_2O exchange f methyl group at 52.52 ppm. Loss of carbamate functional group and methyl group is indicated in ^{13}C NMR spectra by absence of peak at 155 ppm and at 52.52 ppm. An IR spectrum indicates formation of secondary amino group at 3329 cm^{-1} and absence of carbamate peak at 1688cm^{-1}.

DP1 is formed from RIO by bimolecular addition elimination reaction. Based on the above, DP1 is characterised as 2-(1-(2-fluorobenzyl)-1H-pyrazolo[3,4-b]pyridin-3-yl)-N5-methylpyrimidine-4,5,6-triamine.

Mass spectra of DP2 indicates protonated molecular ion at m/z 391. DP2 has 32 amu less than that of RIO. ^{1}H NMR spectra shows absence of one of the methyl protons , there is formation of –NH(-NHCO) at 11.6 ppm. There is loss of carbamate group and formation of imidazolinone at 152.52 ppm, loss of one of the methyl group is indicated by at absence of peak 52.52 ppm. An IR spectrum of DP2 indicates presence of secondary amine at 3282 cm^{-1}. Formation of carbonyl group is indicated by formation of peak at 1710 cm^{-1}. DP2 may be formed by intramolecular cyclisation of $–NH_2$ group and carbonyl group of methyl acetate with the loss of methyl group. DP2 is characterized as 2-(1-(2-fluorobenzyl)-1H-pyrazolo[3,4-b]pyridin-3-yl)-6-amino-7-methyl-7H-purin-8(9H)-one.

A mass spectrum of DP3 indicates that it has 16amu more than that of RIO. In ^{1}HNMR spectra of DP3, in protons of pyridine ring chemical shift is observed in three protons compared to RIO which indicates that formation of N-oxide has taken place in pyridine ring and there is chemical shift value in these protons. IR spectra of DP3 (Fig. 9.52)indicates broad peak in region 3371, 3261, 3010 cm^{-1} indicating the presence of primary, secondary amine, aromatic group and N-oxide. DP3 is

characterized as methyl 2-(1-(2-fluorobenzyl)-1H-pyrazolo[3,4-b]pyridin-3-yl)-4,6-diaminopyrimidin-5-ylmethylcarbamate-N-oxide.

8.7. SECTION - D

IMPURITY PROFILING AND DEGRADATION STUDY OF RIOCIGUAT

8.7.1. EXPERIMENTAL

8.7.1.1. Chemicals and reagents

Chemicals and reagents used in the present section as same as those mentioned in 8.4.1.1.

8.7.1.2. Equipments and Chromatographic conditions

The equipments and chromatographic conditions used in impurity profiling and degradation study are same as those in mentioned in section 8.4.1.3.

For LC-HR-MS analysis , RIO degradation samples were analysed in same chromatographic conditions as mentioned in section 8.4.1.3.The m/z values were determined in both positive and negative ESI mode. On the basis of molecular weight, structures of DPs were proposed and degradation pathway was postulated.

8.7.1.3. Preparation of stock, sample and buffer solutions

Stock, sample and buffer solutions were prepared in the same was as mentioned in section 8.4.1.5.

8.7.2. RESULTS

8.7.2.1. LC-PDA Study

Forced degradation study of RIO showed the formation of degradation products in LC-PDA and are summarized in Table 8.21. Significant degradation was observed in alkaline and slight degradation was observed in oxidative conditions. Degradation products in alkaline and oxidative conditions were identified by LC-HRMS/MS.

Table 8. 21- Summary of forced degradation study of RIO

Stress Condition	Condition	RT of Degradation Products	% of Degradation Products in API	% of Degradation products in formulation
Acid	1M HCl 80ºC for 12 hrs	---	---	---
Alkaline	0.5 M NaOH 60ºC for 1 hr	8.9min (DP2) 11.4 min (DP1)	23.8%	22.3%
Neutral	80ºC for 12 hrs	--	--	--
Oxidative	10 % H_2O_2 RT for 2 hrs	4.0 min(DP3)	9.8%	11.1%
Thermal	80ºC for 11 days	--	--	--
Photolytic Dry	5382 Lux and 144UW/cm^2 for 11 days	--	--	--
Photolytic Solution		--	--	--

8.7.2.2. LC-MS study and characterization of DPs

RIO (m/z 423)

ESI-MS/MS spectra is provided in Fig.8.27a and proposed fragmentation pathway is shown in Fig. 8.27 b. Mass spectral interpretation of RIO is mentioned in section 8.6.2.1.1.

***DP1 (m/z 365*)**

ESI-MS/MS spectra is provided in Fig.8.32 a and proposed fragmentation pathway is shown in Fig. 8.32 b. Mass spectral interpretation of DP1 is mentioned in section 8.6.2.1.2.

DP2 (m/z 391)

ESI-MS/MS spectra is provided in Fig.8.37 a and proposed fragmentation pathway is shown in Fig.8.37 b. Mass spectral interpretation of DP2 is mentioned in section 8.6.2.1.3.

DP3 (m/z 439)

ESI-MS/MS spectra is provided in Fig. 8.42 a and proposed fragmentation pathway is shown in Fig. 8.42 b. Mass spectral interpretation of DP2 is mentioned in section 8.6.2.1.4.

8.7.2.3. Degradation pathway of RIO

The chemical structure of RIO contains pyridine ring fused with pyrazole ring, flurobenzene ring, pyrimidine ring and N-methyl carbamate. Carbamate group is susceptible to hydrolysis. DP1 and DP2 are formed under alkaline condition. DP1 is formed by bimolecular addition reaction under alkaline condition. There is addition of nucleophile hydroxide followed by elimination of methyl group and carbamate group. DP2 is formed by loss of methoxy group and as a result there is cyclisation between carbonyl group and amino group of pyrimidine ring and formation of DP2.Under oxidative condition, there is formation of N-oxide and there is formation of DP3 (Fig.8.47).

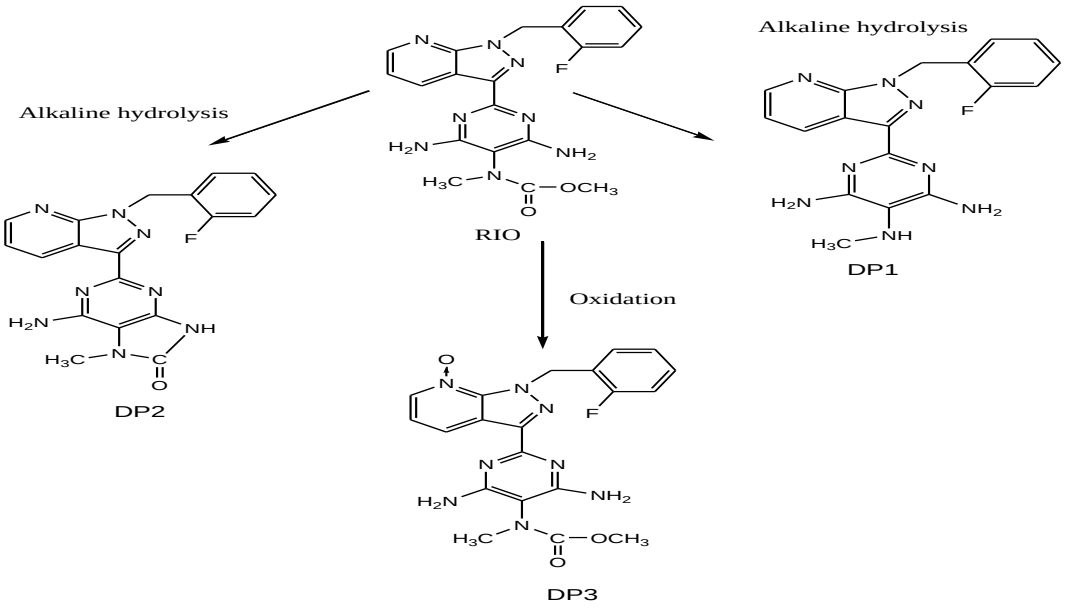

Fig. 8. 47- Degradation pathway of RIO

Table 8. 22 - Chemical structures of RIO and its degradation products

Analyte	Structure	Molecular Formula Molecular Weight Fragments(m/z)	Degradation Route	Rt (LC-PDA)
RIO	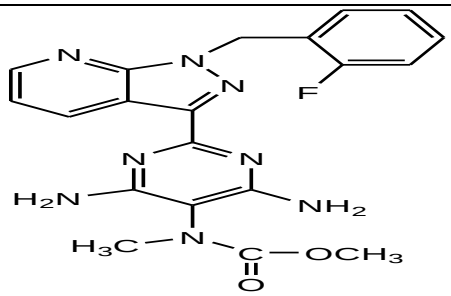 methyl N-[4,6-diamino-2-[1-[(2-fluorophenyl)methyl]pyrazolo[3,4-b]pyridin-3-yl]pyrimidin-5-yl]-N-methylcarbamate	422.42 g,$C_{20}H_{19}FN_8O_2$, Fragments – 391, 109		12.44 min
DP1	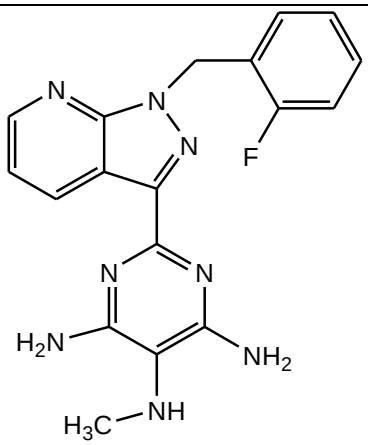 2-(1-(2-fluorobenzyl)-1H-pyrazolo[3,4-b]pyridin-3-yl)-N5-methylpyrimidine-4,5,6-triamine	364.37g, $C_{18}H_{17}FN_8$, Fragments – 256,241, 214, 109	Alkaline	11.4 min

DP2	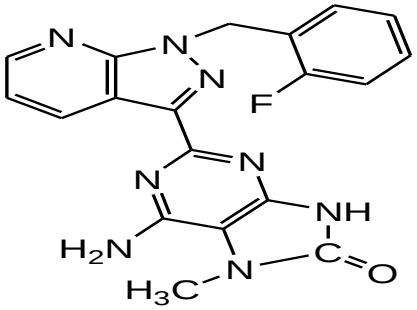 2-(1-(2-fluorobenzyl)-1H-pyrazolo[3,4-b]pyridin-3-yl)-6-amino-7-methyl-7H-purin-8(9H)-one	390.3738, $C_{19}H_{15}FN_8O$, Fragments – 149, 109	Alkaline	8.9 min
DP3	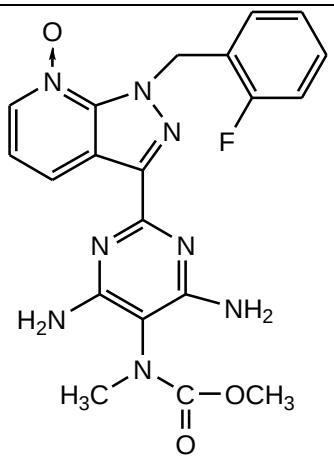 methyl 2-(1-(2-fluorobenzyl)-1H-pyrazolo[3,4-b]pyridin-3-yl)-4,6-diaminopyrimidin-5-ylmethylcarbamate-N-oxide	438.41g, $C_{20}H_{19}FN_8O_3$, Fragments – 422, 390	Oxidative	4.0 min

8.7.3. DISCUSSIONS

Two degradation products in alkaline conditions and one degradation product in oxidative conditions were identified by LC-HR-MS/MS. DP1 and DP2 are formed in alkaline while DP3 is formed in oxidative condition. Details of RIO and its degradation products are given in Table 8.22.

8.8. CONCLUSION

Stability indicating method was developed for determination of Riociguat by HPLC. Significant degradation was observed in alkaline and slight degradation was observed in oxidative condition while Riociguat was stable in acidic, neutral hydrolytic, photolytic and thermal condition. The developed method was validated as per ICH guidelines. Degradation products in oxidative and alkaline conditions were identified by LC-HR-MS/MS. Alkaline degradation follows first-order kinetics. Two degradation products in alkaline and one degradation product in oxidative condition were isolated and characterized by mass, NMR and IR techniques. The degradation pathway in alkaline and oxidative condition was postulated. The three degradation products are hitherto unreported.

8.9. REFERENCES

1. https://pubchem.ncbi.nlm.nih.gov./compound/11304743 (accessed on Apr.11, 2019).
2. https://www.drugbank.ca/drugs/DB08931 (accessed on Apr. 11, 2019).
3. Ghofrani HA, D'Armini AM, Grimminger F, Hoeper MM, Jansa P, Kim NH et al. Riociguat for the treatment of chronic thromboembolic pulmonary hypertension. New England Journal of Medicine. 2013; 369 (4): 319-329.
4. Rubin LJ, Galie N, Grimminger F, Grunig E, Humbert M, Jing ZC et al. Riociguat for the treatment of pulmonary arterial hypertension: a long-term extension study (Patent-2).The European Respiratory Journal. 2015; 45(5): 1211-1213.
5. https://www.accessdata.dfa.gov/drugsatfda_docs/label/2017/204819s006
6. Hill NS, Rahagahi FF, Sood N, Frey N, Ghofrani HA. Individual dose adjustment of riociguat in patients with pulmonary arterial hypertension and chronic thromboembolic pulmonary hypertension. Respiratory Medicine. 2017; 129: 124-129.
7. Chakravarthy AV, Sailaja BV, Praveen K. Method development and validation of ultraviolet-visible spectroscopic method for the estimation of assay of sugammadex sodium, apremilast, riociguat and vorapaxar sulphate drugs in active pharmaceutical ingredient form. Asian Journal of Pharmaceutical and Clinical Research. 2017; 10 (2): 241-250.

8. Temigire PR, Sobia G, Muniipalli VK, Warde S, Singh RM, Nayak S et al. Development and validation of reverse-phase high performance liquid chromatography method for quantitative estimation of riociguat in tablet dosage form. Journal of Pharmacy Research. 2017; 12 (4): 461-465.
9. Meyynathan SN, Nayak R, Narenderan ST, Sai Krishna LV, Kalaivani M, Basvan B. Analytical method development and validation for the determination of Riociguat in their formulations by LC-MS/MS. Journal of Global Pharma Technology. 2018; 10 (12): 19-23.
10. Gnoth NJ, Hopfe PM, Czembor W. Determination of riociguat and its major human metabolite M-1 in human plasma by stable-isotope dilution LCMS/MS. Bioanalysis. 2015; 7 (2) : 193-205.
11. ICH. Impurities in new drug substances Q3A(R2), in: International Conference on Harmonisation,IFMPA, Geneva, Switzerland, 2003.
12. ICH. Impurities in new drug products Q3B(R2), in: International Conference on Harmonisation, IFMPA, Geneva, Switzerland, 2003.
13. Bhutani H, Kurmi M, Singh S, Beg S, Singh B. Quality by design in analytical sciences an overview. Pharma Times. 2014; 46(8): 71-75.
14. Schimdt AH, Stanic M, Molnar I. In silico robustness testing of a compendia HPLC purity method by using a multidimensional design space build by chromatography modeling-case study pramipexole Journal of Pharmaceutical and Biomedical Analysis.2014;91: 97-107.